Science
AAAS

Supplementary Materials for

Csx28 is a membrane pore that enhances CRISPR-Cas13b–dependent antiphage defense

Arica R. VanderWal *et al*.

Corresponding author: Mitchell R. O'Connell, mitchell_oconnell@urmc.rochester.edu

Science **380**, 410 (2023)
DOI: 10.1126/science.abm1184

The PDF file includes:

Materials and Methods
Supplementary Text
Figs. S1 to S22
Tables S1 to S3
References

Other Supplementary Material for this manuscript includes the following:

MDAR Reproducibility Checklist

Materials and Methods

Bacterial Strains and Phages

E. coli C3000 (ATCC 15597) were grown in LB or 1.5% LB agar at 37 °C shaking at 200 rpm. Whenever applicable, media were supplemented with ampicillin (50 μg ml^{-1}) and/or chloramphenicol (15 μg ml^{-1}) to ensure the maintenance of plasmids. C3000 cells were used to propagate MS2 phage (ATCC 15597-B1) according to ATCC recommended handling procedure. *E. coli* MG1655 harboring phage λ cI857 bor::kanR (a heat inducible mutant prophage; (*33*)) were grown in LB supplemented with 10 mM $MgCl_2$ and kanamycin (50 μg ml^{-1}) at 30 °C shaking at 200 rpm until an OD of 0.4. The temperature was increased to 42 °C to elicit the lytic response of the phage which required ~2 hours for complete clearance of the medium. λ-phage was then purified using a previously published protocol (*34*) and stored in SM buffer (50 mM Tris-Cl pH 7.5, 100 mM NaCl, 8 mM $MgSO_4$) at 4 °C. *E. coli* Rosetta2 (DE3) pLysS (Novagen) transformants were grown in terrific broth (TB) at 37 °C shaking at 180 rpm with ampicillin (50 μg ml^{-1}) and chloramphenicol (15 μg ml^{-1}) to ensure the maintenance of plasmids.

Plasmid Construction

Csx28 and Cas13b plasmids in this study are modified versions of the following Addgene plasmids #89909 and #89906, respectively (Table S2 and S3). These plasmids were modified to include a lac operator sequence which is necessary for functional lac operon induction in the presence of IPTG and suppression in the presence of glucose. Additionally, crRNA spacer sequences were inserted between direct repeats at the BsaI restriction site of Cas13b plasmids (Table S2 and S3). Mutants of Csx28 and Cas13b were generated via site-directed mutagenesis (Table S2 and S3).

Efficiency of Plating (EOP)

λ phage was titrated by ten-fold serial dilutions in phage SM buffer. 2 μl of each serial dilution were spotted onto solidified 0.75% top LB agar (LBA) containing 200 μl *E. coli* culture (pre-grown in 5 ml LB overnight) in 3 ml top LBA. Plates were incubated at 37 °C for 16 hours. Plaques were counted and titer was determined as plaque forming units (pfu) ml^{-1}. EOP was calculated as (pfu ml^{-1} (test strain)/pfu ml^{-1} (control strain, *E. coli* C3000)). All experiments include three individual biological repeats with each including technical replicates in triplicate. Csx28 and Cas13b and plasmid mutants were transformed into *E. coli* C3000 prior to plating. For some Cas13b-crRNA-X + Csx28 samples, an uncountable number of plaques were present in the previous dilution but offered no countable plaques on the subsequent dilution; therefore, in these cases, the titer is calculated as one plaque for the subsequent dilution. Statistical significance was calculated using one-way ANOVA and Dunnett's multiple comparisons test with GraphPad Prism 9, comparing strains with plasmids to the untransformed control. No significance was detected, unless indicated ($*p \leq 0.05$). Data was plotted using GraphPad Prism 9.

One-step Phage Growth Curves

Overnight solutions of *E. coli* were used to inoculate 20 ml cultures of LB+10mM $MgCl_2$ at a starting OD_{600} of 0.1 and were grown to OD_{600} of 0.4 when they were infected with λ phage at an MOI of 0.1. Adsorption was carried out for 5 minutes, followed by three 20ml washes with LB+10 mM $MgCl_2$ to remove "free" unabsorbed phage. Pellets were resuspended in 20 ml LB+10 mM $MgCl_2$. For the 0 minute time point (Efficiency of Center of Infection, ECOI), two 100μl aliquots were taken immediately: one serially diluted in LB+10 mM $MgCl_2$ (untreated

sample) and plated directly on top LBA with susceptible host *E. coli*, and the other 100 µl aliquot was treated with a 2% chloroform LB+10 mM $MgCl_2$ solution (treated sample; chloroform lyses the cells and results in only the measurement of mature phage) for 2-3 minutes and then serially diluted in LB+10 mM $MgCl_2$ and plated on top LBA with *E. coli*. Subsequent time points were subjected to only chloroform treatment and titrated in the same manner. At each time point, the pfu ml^{-1} was determined for each strain with the titer representing the number of infectious centers formed. The ECOI was calculated from the untreated sample at 0 minutes as (pfu ml^{-1} (test strain)/pfu ml^{-1} (control strain, *E. coli*)). For each strain and time point, phage titers were performed for three biological replicates and three technical replicates per biological replicate. For statistical analysis, we performed Repeated Measures (RM) one-way ANOVA with Geisser-Greenhouse correction followed by Dunnett's multiple comparisons tests, comparing strains with plasmids to the untransformed control. Individual variances across time points were calculated for each strain. Data was plotted using GraphPad Prism 9.

Bacterial Growth Curves

Overnight cultures of *E. coli* C3000 with plasmids pEmpty, Cas13b, and/or Csx28 or negative controls (untransformed *E. coli and E. coli* with both empty plasmids) were diluted to a final OD_{600} 0.1 in LB+10 mM $MgCl_2$ supplemented with ampicillin and chloramphenicol in presence of λ phage for a final MOI of 0, 0.2 and 2. 200 µl of the mixed samples were transferred into wells of a 96-well plate in triplicate. Plates were incubated at 37 °C with shaking in a Tecan Spark plate reader with A_{600} measurements taken every 10 minutes with the first time point at 0 minutes. Data was plotted using GraphPad Prism 9.

Colony Forming Unit and Lysogeny Assay

Cells were prepared as described above for bacterial growth curves. At the end of the growth curve (400 minutes), cells were collected with 3 replicates per sample. Serial dilutions of each sample were made in SM buffer with 4 µl of each dilution spotted onto LB agar plates in triplicate. To estimate all viable cells, untransformed *E. coli* sample dilutions were spotted onto LB only plates and transformed *E. coli* sample dilutions were spotted onto LB supplemented with ampicillin and chloramphenicol. In parallel, to estimate the number of viable lysogenic cells, samples were spotted onto LB agar plates supplemented with kanamycin to select for the resistance marker in λ cI857 bor::kanR. All agar plates were incubated at 37 °C overnight. Resulting colonies were counted to calculate colony forming units per milliliter (CFU) for each sample condition. The fraction of lysogenic colonies was then determined by dividing the lysogenic CFU by the corresponding total CFU. Statistical significance was calculated using multiple unpaired t tests with GraphPad Prism 9, comparing each sample against the corresponding MOI of untransformed control. No significance was detected, unless indicated ($*p \leq 0.05$). Data was plotted using GraphPad Prism 9.

Csx28 Protein Expression and Purification

The Csx28 expression vector was assembled by using a PCR fragment of the PbuCsx28 ORF from the PbuCsx28 Addgene plasmid (#89909; Table S2). Csx28 was C-terminally tagged with a TEV-MBP-His6 cleavage site sequence with expression driven by a T7 promoter. Expression vectors were transformed into Rosetta2 (DE3) pLysS *E. coli* cells and grown in TB broth at 37 °C, induced at mid-log phase with 0.5 mM IPTG, and grown for an additional three hours until harvested. Cell pellets were resuspended in lysis buffer (50 mM HEPES pH 7.5, 1 M NaCl, 5% glycerol, 1 mM TCEP, 1% DDM, 20mM imidazole, and EDTA-free protease inhibitor (Roche)),

lysed by sonication, and clarified by centrifugation at 16,000g. Soluble Csx28-TEV-MBP-His6 was isolated over metal ion affinity chromatography and rinsed with wash buffer (50mM HEPES pH 7.5, 1 M NaCl, 5% glycerol, 1 mM TCEP, 0.1% DDM, and 40mM imidazole) and eluted in elution buffer (50mM HEPES pH 7.5, 1 M NaCl, 5% glycerol, 1 mM TCEP, 0.1% DDM, and 300mM imidazole). Eluate was treated with TEV protease at 4 °C during overnight dialysis in dialysis buffer (50mM HEPES pH 7.5, 500 mM NaCl, 5% glycerol, and 1 mM TCEP) to remove the MBP-His6 tag. Cleaved protein was loaded onto a second metal ion affinity column to clear the MBP-His6 tag. Csx28 eluate was concentrated and further purified via size-exclusion chromatography on a Superdex 200 Increase 10/300 GL column (Cytiva) column equilibrated with 20mM HEPES pH 7.5, 200 mM KCl, 1 mM TCEP, 5% glycerol, and 0.1% DDM and stored at −80 °C. Size exclusion chromatography traces were plotted using GraphPad Prism 9.

Static Light Scattering Size Exclusion Chromatography (SEC-SLS)

Purified Csx28 was loaded onto a Superdex 200 Increase 10/300 GL column (Cytiva) in-line with UV (Postnova Analytics), static light scattering and refractive index detectors (Precision Detectors), pre-equilibrated with a buffer containing 20mM HEPES pH 7.5, 200 mM KCl, 1 mM TCEP, 5% glycerol, and 0.1% DDM. Data were collected using (PrecisionAcquire32 and PrecisionDiscovery32, Precision Detectors), and molecular masses were calculated using manually normalized values and the three detector method (*35*) using BSA as a known molecular mass control. Data was plotted using GraphPad Prism 9.

In vitro Protein Crosslinking

In vitro protein crosslinking was performed using bis[sulfosuccinimidyl] glutarate-d_0 (BS^2G-d_0, spacer arm length 7.7 Å, ThermoFisher Scientific) as suggested by the manufacturer. Briefly, water/DMSO control or crosslinker in 10- or 50-fold molar excess were added to Csx28 light or heavy fraction (final Csx28 concentration 5 μM) in crosslinking reactions containing 20 mM HEPES buffer pH 7.5 and incubated at room temperature. Aliquots were removed at 0 and 15 minutes and reactions were terminated by addition of 1M NH_4NCO_3 to a final concentration of 20 mM. Then equivalent volumes of crosslinking reactions were denatured in SDS-loading buffer at 95 °C for 10 minutes, loaded onto NuPAGE Bis-Tris 4-12% gradient gel (Invitrogen), samples separated at 150 V for 90 minutes followed by gel staining with Silver Stain Plus Kit (BioRad).

Cryo-EM Sample Preparation

Graphene-oxide (GO) covered grids were prepared following previously published protocols (*36*), using C-Flat 1.2/1.3 grids (Protochip), and vitrified using a Mark IV Vitrobot (ThermoFisher) at 4°C and 100% humidity. 4 μL of 0.35 mg/mL Csx28 was applied to a freshly prepared GO grid, blotted for 6 seconds and blot force 6, and subsequently plunged into a slurry of liquid ethane cooled using liquid nitrogen.

Cryo-EM Image Processing, Model Building and Structure Prediction

Prepared grids were imaged at 63,000X nominal magnification (1.33Å/pixel) using Talos Arctica (ThermoFisher) equipped with a Gatan K3 direct electron detector (Gatan) and Gatan bioquantum energy filter (GIF, Gatan). Prior to image acquisition, the microscope was carefully aligned according to recommended procedures for coma-free and parallel illumination settings (*37*). A total of 904 micrographs were collected using SerialEM (*38*), 2 by 2 image shift, and

nominal defocus range of -1 μm to -2.5 μm. The total dose was 47 electrons/Å^2 fractionated into 44 frames and a total of 2.96 seconds exposure (Fig. S9A, Table S1). The following pre-processing and micrograph selection steps were carried out using Warp (*39*): beam-induced motion correction, CTF estimation, and particle picking. The final set of 314 micrographs with an estimated resolution of 5 Å or better were imported to cryoSPARC (*40*) for subsequent processing. Template-based particle picking in cryoSPARC resulted in 247,026 particles. 2D classification of this particle set resulted in multiple 2D classes of side-like views and one top-view with 8-fold symmetry, resulting in 118,793 selected particles. *Ab initio* model generation (C1 symmetry) resulted in a reconstruction with clear 8-fold symmetry. Subsequent downstream processing steps were performed while imposing C8 symmetry (Fig. S9B-C).

After non-uniform refinement in cryoSPARC, the particle stack was imported to RELION (*41*) for subsequent refinement. Further rounds of 3D classification resulted in two major classes of Csx28 octamer, and one minor class consisting of two stacked Csx28 octamers (i.e. a dimer of octamers). As two octamer classes didn't show distinct conformational differences, two classes of 111,831 particles were combined for further refinement. Extensive CTF refinement and Bayesian polishing with RELION (*41, 42*) was followed. Subsequent rounds of 3D classification to identify classes with qualitatively high-resolution features improved the final resolution from 4.3 Å to 3.65 Å and 58,694 final particles. Local resolution of the final map was estimated using cryoSPARC (Fig. S9D). Although this final map showed significantly improved overall resolution, N-terminal trans-membrane helixes were better resolved in the initial cryoSPARC reconstruction (from 118,793 particles before rounds of classification in RELION, fig. S6C). The appearance of the N-terminal helices (7 Å+ resolution) is likely due to the liberal masking imposed by the initial cryoSPARC reconstruction (which also includes micelle density, 10 Å) and the comparatively worse resolution of the N-terminal helices (~7 Å) compared to that of the soluble portion (4 – 5 Å) of Csx28 (which was subjected to high-resolution refinement).

The final map was sharpened using RELION postprocess function and automatically estimated B-factor (-118 Å^2). The sharpened map was of sufficient resolution (3.6 Å) for *de novo* model building (as homologous structures were not available). The initial atomic model was manually built using coot (*43*), focusing on a single asymmetric unit. Most of the model (from residue 32 to 171) was built using the final map from RELION, and N-terminal trans-membrane helix (from residue 19 to 31) was built using the initial cryoSPARC reconstruction. The manually built subunit was then manually docked into the density using UCSF Chimera (*44*) in order to create the octameric assembly. This model was subjected to iterative process of manual inspection, followed by manual adjustments using coot (*43*), followed by symmetric refinement using RosettaES (*45*). Model-map FSC (Fig. S9E), EMRinger score (*46*), and MolProbity (*47*) (Table S1) were calculated using Phenix (*48, 49*) model validation tools. AlphaFold (*20*) structure prediction was carried using a ColabFold batch implementation (*50*) using the fast homology search of MMseq2 with AlphaFold2, using the following options: colabfold_batch --amber --templates --num-recycle 3 --model-type AlphaFold2-multimer-v2 (*22*). This analysis was conducted using the computational resources of the University of Rochester's Center for Integrated Research Computing cluster. RoseTTA fold (*21*) predictions were carried out using the Robetta online server (https://robetta.bakerlab.org/), using standard parameters. DeepTMHMM (*51*) transmembrane spanning region predictions were carried out using the DeepTMHMM online server (https://dtu.biolib.com/DeepTMHMM/), using standard parameters. Phylogenetic tree building used to select Csx28 orthologs for DeepTMHMM and AlphaFold analyses was carried out by running six iterations of PSI-BLAST (*52*) to gather 500 PbuCsx28

orthologs, followed by tree building with BLAST Tree View with Fast Minimum Evolution (max seq difference 0.9 using the Grishin Distance Matrix) to visualize protein sequence divergence. iTOL (https://itol.embl.de/) was used for unrooted tree visualization with branch lengths ignored (*53*).

Membrane Fractionation and Western Blotting

For western blot detection, Csx28 and Cas13b plasmids were modified to contain a C-terminal V5 and N-terminal 3xHA epitope tag, respectively. Membrane fractionation was performed as previously described (*54*). Briefly, 300 ml of pEmpty + pACYC184 (ΔCas13 empty control), HA-Cas13b + pEmpty, pACYC184 + Csx28-V5, and HA-Cas13b:crRNA-1 + Csx28-V5 expressing cultures were harvested at OD 0.6, resuspended in 15 ml cell resuspension buffer (50 mM sodium phosphate buffer, 300 mM NaCl, 2 mM $MgCl_2$, 0.2 mg/ml DNaseI, EDTA-free protease inhibitor (Roche) and 0.1 mg/ml lysozyme) and lysed using a French press at 12,000 psi. Lysate was cleared of unbroken cells by centrifugation (12,000 x g) and samples of the supernatant (whole cell lysate) were collected for Western analysis. The lysate was further purified by ultracentrifugation (180,000 x g) which resulted in cytosol (supernatant) and membrane (pellet) fractions. The membrane fraction was resuspended in membrane resuspension buffer (50 mM sodium phosphate buffer, 300 mM NaCl, 5% glycerol, EDTA-free protease inhibitor (Roche), 2% DDM) and was further separated into soluble membrane fraction and insoluble membrane fraction via ultracentrifugation (180,000 x g). Samples from the cytosol, soluble membrane, and insoluble membrane fractions were collected for Western analysis. Sample loading was normalized by running 0.1% of each total fraction volume. Two gels with identical sample loading order and amount were probed and stripped for subsequent probing. HA-Cas13b was detected using monoclonal rat anti-HA antibody (1:1000 in PBST, Roche, Cat # 12013819001) and a goat anti-rat HRP-conjugated secondary antibody (1:3000 in PBST; SeraCare, Cat # 5220-0364). Csx28-V5 was detected by mouse monoclonal anti-V5 antibody (1:5000 in PBST, Invitrogen, Cat # R960-25) and a goat anti-mouse HRP-conjugated secondary antibody (1:3000 in PBST; Santa Cruz Biotechnology, Cat # sc-2357). Cytoplasmic control, DnaK, was detected by polyclonal rabbit anti-DnaK antibody (1:1000 in PBST, Biorybt, Cat # orb53459) and goat anti-rabbit HRP-conjugated secondary antibody (1:3000 in PBST; Santa Cruz Biotechnology, Cat # sc-2004); and membrane control, OmpC, was detected by polyclonal rabbit anti-OmpC antibody (1:1000 in PBST, Biorybt, Cat # orb6940) and a goat anti-rabbit HRP-conjugated secondary antibody (1:3000 in PBST; Santa Cruz Biotechnology, Cat # sc-2004).

Inner and Outer Membrane Fractionation, and Western Blotting

Inner and outer membrane fractionation was performed as previously described (*34*). Briefly, 1 L of pACYC184 + Csx28-V5 and Cas13b:crRNA-1 + Csx28-V5 expressing *E. coli* C3000 cultures were harvested at OD_{600} 1. In addition, a 1 L Cas13b:crRNA-1+Csx28-V5 culture was also inoculated at OD_{600} of 0.1 with λ phage at a MOI of 0.1 and harvested at OD_{600} of 1. All pellets were resuspended in 15 ml cell resuspension buffer (20 mM sodium phosphate buffer pH 7.0, 0.2 mg/ml DNase I, EDTA-free protease inhibitor (Roche), and 0.1 mg/ml lysozyme) and lysed using a French press at 12,000 psi. Lysates were cleared of unbroken cells by centrifugation at 12,000×*g* (4° C) for 10 minutes and samples of the supernatant (whole cell lysate) were collected for Western analysis. The supernatants were further ultra-centrifuged at 180,000×*g* (4° C) for one hour which resulted in cytosolic (supernatant) and membrane (pellet) fractions. The membrane fractions were resuspended in 20 mM sodium phosphate buffer pH 7 and 2% N-

lauroylsarcosine (Sigma-Aldrich) and incubated at 4 °C overnight with rocking to solubilize the inner membrane followed by centrifugation again at 180,000×*g* for one hour. The outer membrane enriched pellet was resuspended in 20 mM sodium phosphate, 50 mM NaCl and 0.5% N-tetradecyl-N,N-dimethyl-3-ammonio-1-propanesulfonate (Sigma-Aldrich) and incubated at 4 °C overnight with rocking. Insoluble materials were removed by a final ultracentrifugation spin at 85,000×*g* for one hour. Samples from the cytosol, inner membrane, and outer membrane fractions were collected for Western blot analysis. Sample loading was normalized by running 0.1% proportions of each total fraction volume. Two gels with identical sample loading order and amounts were transferred to Protran nitrocellulose membranes, tested with one antibody and stripped for subsequent probing with other antibodies. Csx28-V5, Dnak, and OmpC were detected as previously described for membrane fractionation and Western blotting.

In vivo Protein Crosslinking

Protein *in vivo* crosslinking was carried out with membrane-permeable DSS (disuccinimidyl suberate, spacer arm 11.4 Å) (Thermo Scientific) as suggested by the manufacturer. Briefly, 2×10^{10} non-infected or λ phage (MOI:0.1) 1 hr-post infected *E. coli* C3000 expressing V5-tagged Csx28, HA-tagged Cas13 or combination of both proteins together with C3000 host strain as negative control were washed three times in ice-cold 1×PBS (to remove any amine-containing compounds) and treated with 2 mM DSS for 30 minutes at room temperature. Then reactions were quenched by addition of 1 M Tris pH 7.5 to a final concentration 20 mM for 15 minutes at room temperature and cells collected by centrifugation. The status of Csx28 protein in crosslinked cells was determined by making the total cell extracts and carrying out Western blot analysis as described above.

Cell Extract Fractionation using Glycerol Density Gradients

30 ml cultures of uninfected or 90 minutes post λ-phage (MOI: 0.1) infected *E. coli* C3000 expressing tagged Csx28-V5 and Cas13:crRNA-1 were pelleted and washed with 1×PBS buffer. Cell extracts were prepared by resuspending cell pellets in buffer containing 20 mM HEPES pH 7.5, 200 mM KCl, 5 mM $MgCl_2$, 5% glycerol, 0.5 mg/ml lysozyme and incubating for 20 minutes at room temperature followed by lysis with the addition of Triton X-100 to final concentration of 0.5% in presence of EDTA-free protease inhibitors (Roche Applied Science), DNase I and RNase A (both at 0.1 mg/ml final concentration, Sigma-Aldrich). After a 15 minute incubation, the cell extracts were centrifuged in cold microcentrifuge at 10,000×*g* for 10 minutes. Supernatants (equivalents of 500 µg) were loaded on the top of 11 ml linear 5–45% glycerol gradients prepared in cell extract buffer, centrifuged in SW41 rotor at 39,000 rpm, 5 °C for 16 hours and 500 µl fractions were collected from the bottom of each gradient. The absorbance at 280 and 260 nm was determined for each fraction to monitor the gradient density reproducibility. The aliquots of every second fraction were loaded onto NuPAGE Bis-Tris 4-12% gradient gels (Invitrogen), followed by separation at 150 V for 90 minutes and Western blotting using Protran nitrocellulose membranes, pore size 0.1 µm (Cytiva). Membranes were probed with anti-V5 mouse monoclonal antibody (Invitrogen) followed by treatment with goat anti-mouse HRP-conjugated secondary antibody (Santa Cruz) and ECL-reagents (SuperSignal West Pico PLUS, ThermoFisher Scientific) before visualization on a BioRad Gel Doc XR Imaging System to determine the sedimentation distribution of Csx28 in the density gradients.

Flow Cytometry

Overnight cultures of *E. coli* C3000 expressing Csx28 and/or Cas13:crRNA-1 or appropriate controls in LB media were diluted to OD 0.1 and grown until OD 0.4, at this time cells were infected with λ-phage at an MOI of 1 and 10 mM $MgCl_2$ was added to the media. 200 µl samples were collected at time 0 , 30-, and 90-minutes post infection. Samples were treated with the fluorescent voltage sensitive dye DiBAC4(3) (5 µM) for 10 minutes at 37 °C. Treated cells were then pelleted and washed with fresh LB+10mM $MgCl_2$ twice and finally diluted 1:10 in fresh LB+10 mM $MgCl_2$. Samples were measured using a Cytek Aurora Full Spectrum Flow Cytometer measuring 100,000 events (cells) per sample and data were analyzed using FCS Express7 Research (De Novo Software) and data was plotted using GraphPad Prism 9.

Resazurin Assays

E. coli C3000 cultures expressing Csx28 and/or Cas13:crRNA-1 or appropriate controls were prepared as described above for bacterial growth curves with the exception that assay was paused after 1 hour post λ-phage infection to allow for resazurin addition. Resazurin (final concentration 3 µg/ml; stock dissolved in PBS, pH 7.4, 0.2 µm filtered sterilized) was added to each 200 µl sample-containing well in addition to three wells of LB media control, the assay was resumed with fluorescent measurements taken every 10 minutes with 560 nm excitation / 590 nm emission wavelengths using a Tecan Spark plate reader.

RNA Electrophoretic Mobility Shift Assays (EMSA)

Purified Csx28 protein (light and heavy fraction) and fluorescein-labeled RNA oligonucleotide (EMSA_RNA; Table S3) were assembled in 10 µl reactions containing the following buffer: 20 mM HEPES pH 7.5, 50 mM KCl, 5 mM $MgCl_2$, 5% glycerol, 0.1% DDM, and 1mM TCEP. Each reaction contained 1 pmol of RNA and serially diluted protein ranging from molar ratio 2:1 (excess of RNA) to 1:16 (excess of protein), respectively. Reactions were incubated for 60 minutes at 37 ° C. Complexes assembled in each reaction condition were resolved on an 8% native PAGE gel using Tris-Borate-EDTA running buffer at 150 V for 90 minutes at 4 °C. Positions of FAM-labeled RNA in the samples on a gel were visualized using a Typhoon™ RGB Imager (GE Healthcare) using Cy2 filter, emission wavelength range 515 to 535 nm, excitation wavelength 488 nm.

In vitro Protein-RNA Crosslinking

1 or 2 µg of Csx28 (heavy fraction) was assembled with RNA (crosslink_RNA; Table S3; IDT) at 1:1 molar ratio in 1×PBS buffer containing 0.1% NP-40 at 37° C for 15 minutes and then reactions cooled on ice. Three independent reactions of assembled complexes were then UV-irradiated in quartz cuvettes using UV Stratalinker 1800 (wavelength 254 nm, Agilent/former Stratagene) at 120,000 microjoules/cm^2. The Csx28 cross-linked products were denatured in SDS-loading buffer at 95 °C for 10 minutes, loaded onto NuPAGE Bis-Tris 4-12% gradient gel (Invitrogen), followed by sample separation at 150 V for 90 minutes and gel staining with Silver Stain Plus Kit (BioRad).

Fluorescent RNA Cleavage Assay

PbuCas13b was purified and crRNA (Pbu_Cas13b_crRNA_A; Table S3) and target-RNA (Target_RNA_A; Table S4) were prepared as previously described (*2*). PbuCas13b:crRNA complexes were preassembled by incubating 1 µM of PbuCas13b with 1.1 µM nM of crRNA for

2 minutes at 37 °C, followed by 8 minutes at room temperature, followed by placing on ice. These complexes were then diluted to 100 nM PbuCas13b, 110 nM crRNA, in the following buffer (20 mM HEPES pH 7.5, 50 mM KCl, 5 mM $MgCl_2$, 5% glycerol (v/v), 0.1% DDM (w/v), 1mM TCEP in the presence of 150 nM of RNAase-Alert fluorescent RNA substrate (Thermo-Fisher), and the absence or presence target-RNA (100 nM) and/or PbuCsx28 (heavy or light fraction; 100 nM). These reactions were incubated in a fluorescence plate reader (Tecan Spark) for 1 hour at 37 °C with an endpoint reading at 1 hour (λex: 485 nm; λem: 535 nm). Maximal fluorescence was measured by incubating 50 nM RNase A with 150 nM of RNAase-Alert substrate. The data was plotted using GraphPad Prism 9.

Total RNA Sample Analysis using Bioanalyzer

5 ml *E. coli* C3000 cultures expressing Csx28 and/or Cas13:crRNA-1 or appropriate control cultures (uninfected or 180 minutes after λ-phage infection [MOI:0.2]) were immediately flash frozen in liquid nitrogen and stored at -80° C overnight at the time of collection. For processing, each culture was quickly thawed in ice water and pelleted in a cold centrifuge. Cell pellets were used to prepare total RNA with *mir*Vana™ miRNA Isolation Kit, with phenol (Ambion) as suggested by manufacturer for total RNA preparation. Obtained RNA was evaluated for concentration and quality by using NanoDrop One instrument (ThermoFisher Scientific), then samples were subjected for analysis using 2100 Bioanalyzer Instrument and Total RNA 6000 Pico chip (Agilent). RNA sample results were processed using Agilent 2100 Expert Software and bioanalyzeR (v. 0.9.2; https://github.com/jwfoley/bioanalyzeR) and the data was plotted in GraphPad Prism 9.

Protein Immunoprecipitations and Western Blotting

100 ml *E. coli* C3000 cultures expressing Csx28-V5 and/or Cas13b-HA:crRNA-1 or appropriate control cultures (uninfected or 90 minutes after λ-phage infection; MOI: 0.1) strains were pelleted by centrifugation, washed in cold 1×PBS buffer, cell pellet resuspended in small volume of 1×TE and treated with lysozyme (0.5 mg/ml final concentration) for 15 minutes at room temperature. Next cells were lysed in a buffer containing 50 mM HEPES pH 7.5, 140mM KCl, 1% Triton X-100, 0.25% sodium deoxycholate, 0.1% sodium dodecyl sulfate and EDTA-free protease inhibitors (Roche) for 20 minutes on ice followed by treatment with DNase I for 10 minutes at RT. Cell lysate suspensions were pelleted at 10 minutes at 10,000 ×*g* in cold centrifuge and supernatants were used in immunoprecipitation experiments (with small aliquots of supernatants saved as loading controls). For Csx28-V5 tagged protein immunoprecipitation 15 µl of mouse monoclonal anti-V5 antibody (Invitrogen) was added to each cell extract and mixtures were incubated at 4°C for 2 hours with rotation followed by the addition of 30 µl of Protein A/G magnetic beads (ThermoFisher Scientific) and incubation for an additional hour at 4°C. Magnetic bead separation was performed using DynaMag™-2 Magnet magnetic stand (ThermoFisher Scientific) first by removing unbound material, followed by three washes: two containing 1× cell lysis buffer and one in between including 1× cell lysis buffer with 1M NaCl. Bound proteins were eluted from magnetic beads by treating them in 30 µl of 0.1 M glycine pH 2.0 for 10 minutes at RT and separating on magnetic stand. Aliquots of eluted proteins were denatured in 1×SDS loading buffer at 95°C for 10 minutes and loaded onto NuPAGE Bis-Tris 4-12% gradient gels (Invitrogen) together with aliquots of cell extracts, followed by separation at 150 V for 90 minutes, Western blotting to nitrocellulose membrane and probing with rat anti-HA antibody (Roche) and mouse anti-V5 antibody (Invitrogen), as described above for the Glycerol Gradient Fractionation assay. A similar procedure was used to immunoprecipitate HA-Cas13b

protein from cell extracts except that immunoprecipitation was performed in one step using the anti-HA magnetic beads (ThermoFisher Scientific).

Analytical Size Exclusion Chromatography

Analytical size exclusion chromatography was conducted on an ÄKTA pure purification system (Cytiva). Cas13b, crRNA, and/or target RNA (heavy fraction) Samples were prepared at a molar ratio of 1:1:1 and incubated at 10 minutes at 37 °C prior to the addition of 8 molar equivalents of Csx28 monomer (to account for octamer formation), incubated for a further 30 minutes at 37 °C before loading a loaded onto a Superdex 200 Increase 10/300 GL column (Cytiva) equilibrated with 20mM HEPES pH 7.5, 200 mM KCl, 1 mM TCEP, 5% glycerol, and 0.1% DDM. Eluates were monitored by absorbance at 260 and 280 nm. Size exclusion chromatography traces were plotted using GraphPad Prism 9.

Supplementary Text

Colony forming units and lysogen formation assays

To ensure the cell density measurements weren't an artefact of a change in cell morphology, we carried out complementary colony-forming unit assays and observed an increase in cell numbers upon Cas13b-mediated activation of Csx28 anti-phage defense (Fig. S4A). Concurrently, we were also curious whether Csx28 activation affects λ-phage's ability to lysogenize our *E. coli* strains (i.e., insert into the genome as prophage), so we carried out colony-forming unit assays in the presence of kanamycin (as our λ-lysogen harbors a kanamycin resistance gene) and observed that Cas13b-mediated activation of Csx28 significantly inhibits lysogen formation at both low and high MOIs (Fig. S4B). This observation is evidence that protection against λ infection is not due to increased lysogen formation but rather that Csx28 offers phage defense beyond preventing lytic destruction of the culture.

Structure prediction across a Csx28 phylogenetic tree

To explore whether N-terminal transmembrane helix formation, and the overall fold and octameric arrangement of Csx28 is broadly conserved across predicted Csx28 orthologs, we selected a sample of 10 orthologs dispersed across a Csx28 phylogenetic tree we constructed (Fig S.11) and carried out DeepTMHMM (*51*) membrane spanning region predictions (Fig S12) and AlphaFold-Multimer (*22*) predictions (Fig S13)., respectively. We observed in all cases that the N-terminus of these orthologs is confidently predicted to be a transmembrane helix, and they all form a very similar overall fold and octameric structure that utilizes the same protomer: promoter interface for oligomer formation, even at very low sequence identities. Taken together, these data provide further evidence that our cryo-EM model likely represents the major structural form of Csx28 found in nature.

In vivo Cas13b RNA cleavage assays

This subtle change in RNA length distributions (Fig. S20B-E) is not surprising given the very modest protection Cas13b:crRNA1 provides against λ-phage in the absence of Csx28 (Fig.1), and recent evidence showing that widespread Cas13 collateral cleavage (vs. Cas13 target-bound cleavage) is highly dependent on the target transcript expression level of the target transcript in *E. coli,* with many Cas13:crRNA target pairs not eliciting collateral cleavage *(55).*

Supplementary Figures

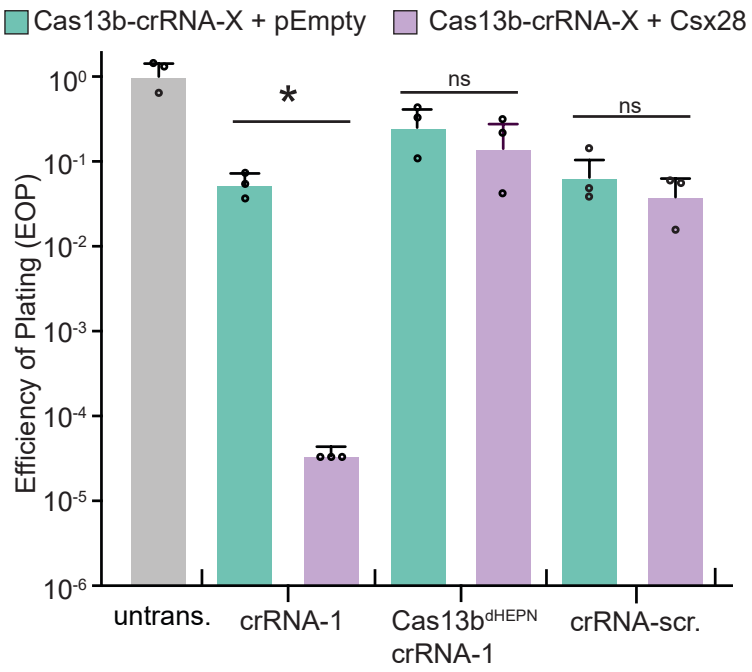


Fig. S1. Csx28 activation requires a nuclease-active and targeting Cas13b:crRNA complex. Efficiency of Plating (EOP) assays measuring λ-phage infection susceptibility of untransformed (untrans.) *E. coli* or strains carrying the indicated Cas13b-crRNA-X, Csx28, or pEmpty plasmids. Cas13b^{dHEPN} is a HEPN-nuclease deactivated Cas13b control and crRNA-scr. is a non-targeting crRNA control generated by scrambling the spacer sequence of crRNA-1. For some Cas13b-crRNA-X + Csx28 samples, an uncountable number of plaques were present in the previous dilution but offered no countable plaques on the subsequent dilution. Therefore, in these cases, the titer is calculated as one plaque for the subsequent dilution. Data is shown as mean ± s.e.m for $n = 3$ biological replicates. Statistical significance was calculated using unpaired t-tests by comparing strains with empty plasmid against those with Csx28 plasmid (*$p<0.05$). Multiple comparisons correction was carried out using the Holm-Šídák method with alpha set to 0.05.

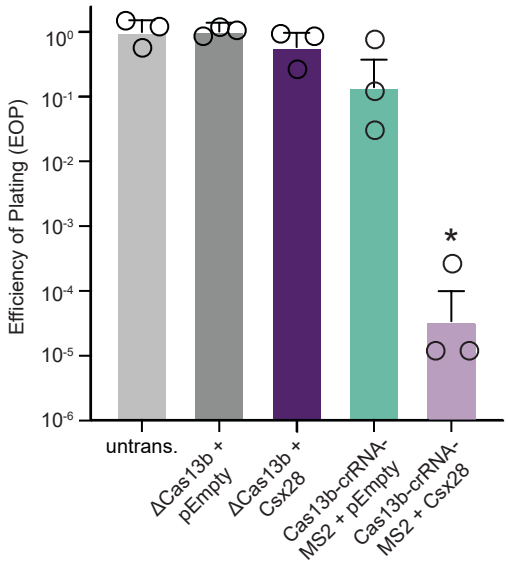


Fig. S2. Csx28 significantly enhances Type VI-B2 CRISPR-Cas immunity against MS2 ssRNA phage and requires targeting Cas13b for this activity. Efficiency of Plating (EOP) assays measuring MS2-phage infection susceptibility of untransformed (untrans.) *E. coli* or strains carrying the indicated Cas13b-crRNA-MS2, Csx28, or pEmpty plasmids. ΔCas13b is no Cas13b (empty plasmid) control. Data is shown as mean ± s.e.m for $n = 3$ biological replicates. For some Cas13b-crRNA-MS2 + Csx28 samples, an uncountable number of plaques were present in the previous dilution but offered no countable plaques on the subsequent dilution. Therefore, in these cases, the titer is calculated as one plaque for the subsequent dilution. Statistical significance was calculated using one-way ANOVA and Dunnett's multiple comparisons test, comparing strains with plasmids to the untransformed control. No significance was detected, unless indicated (*$p \leq 0.05$).

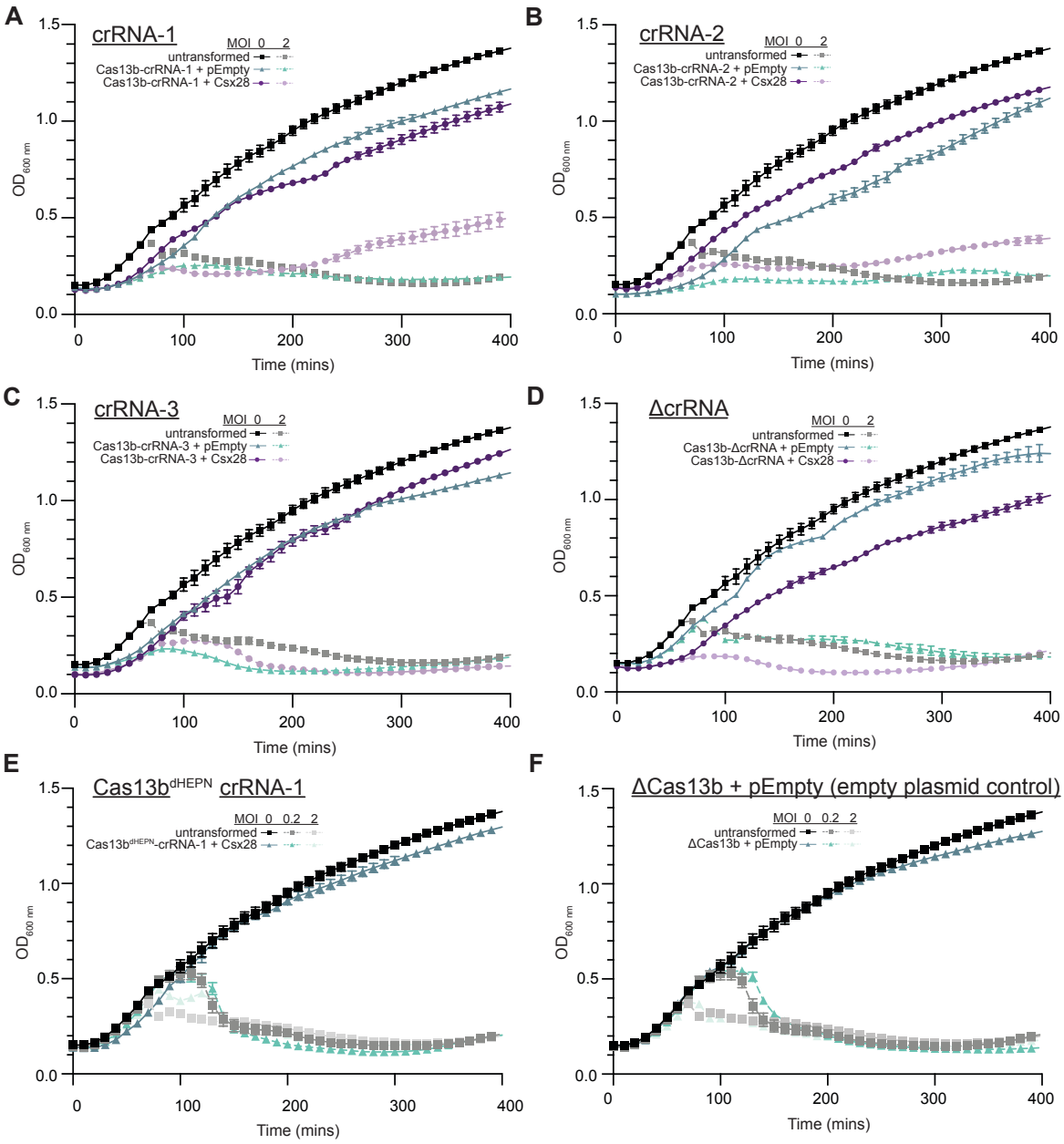


Fig. S3. Cas13-activated Csx28 also allows *E. coli* to continue growth at a reduced rate despite λ-phage infection at high MOI. Growth curves of *E. coli* strains carrying the indicated either untransformed or Cas13b-crRNA-X, Csx28, or pEmpty plasmids, as measured using OD_{600} in the absence or presence of λ-phage at the indicated MOIs. (**A-F**) are growth curves for crRNA-1, crRNA-2, crRNA-3, ΔcrRNA, Cas13b^{dHEPN}:crRNA-1, ΔCas13b + pEmpty containing strains, respectively. Cas13b^{dHEPN} is a HEPN-nuclease deactivated Cas13b control and ΔCas13b is no Cas13b (empty plasmid) control. Data is shown as mean ± s.e.m for $n = 3$ biological replicates.

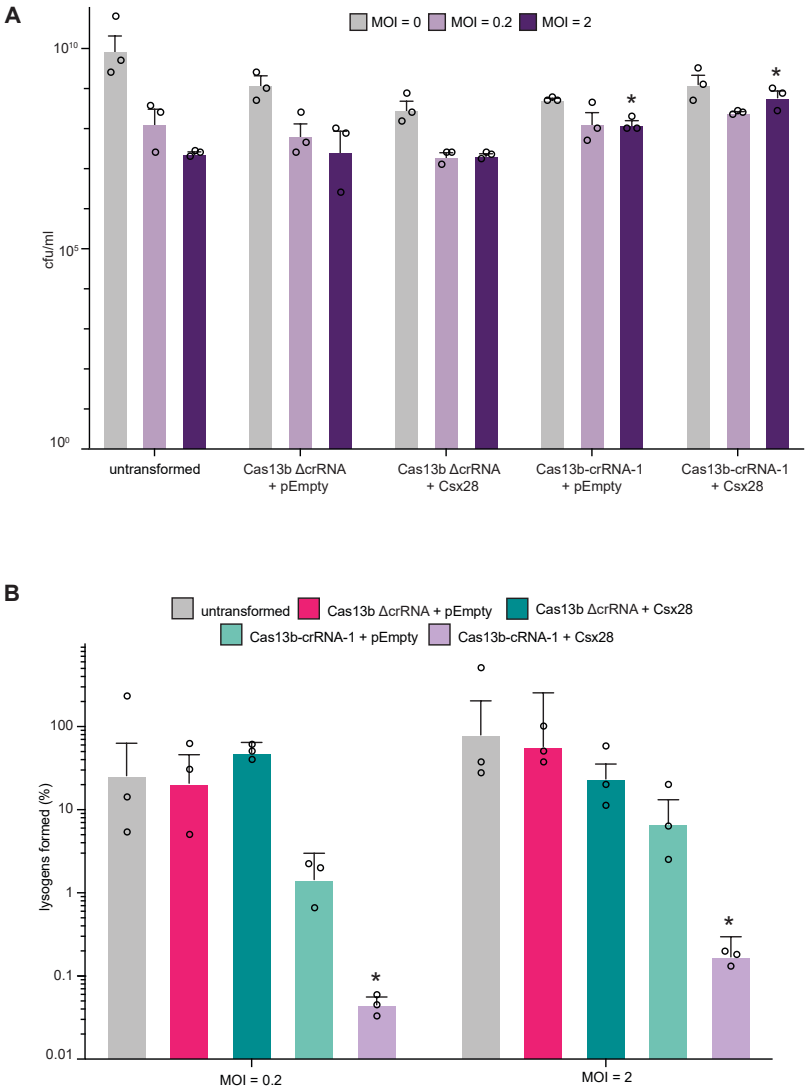


Fig. S4. Cas13b-activated Csx28 reduces loss of colony formation and prevents significant lysogeny upon λ-phage infection at low and high MOIs. (**A**) Colony Forming Unit Assay. *E. coli* strains carrying the indicated either untransformed or Cas13b-crRNA-X, Csx28, or pEmpty plasmids were serially diluted and plated 400 minutes post λ-phage infection (MOI: 0, 0.2, 2). To estimate all viable cells, untransformed *E. coli* sample dilutions were spotted onto LB only plates and transformed *E. coli* sample dilutions were spotted onto LB supplemented with ampicillin and chloramphenicol. (**B**) Lysogen Formation Assays. In parallel, to estimate the number of viable lysogenic cells, samples were spotted onto LB agar plates supplemented with kanamycin to select for the kanamycin resistance marker in λ-phage. Resulting colonies were counted to calculate colony forming units per milliliter (cfu) for each sample condition. The fraction of lysogenic colonies was then determined by dividing the lysogenic cfu by the corresponding total cfu. Data is shown as mean ± s.e.m for $n = 3$ biological replicates. Statistical significance was calculated using multiple unpaired t tests, comparing each sample against the corresponding MOI of untransformed control. No significance was detected, unless indicated (*$p \leq 0.05$). Multiple comparisons correction was carried out using the Holm-Šídák method with alpha set to 0.05.

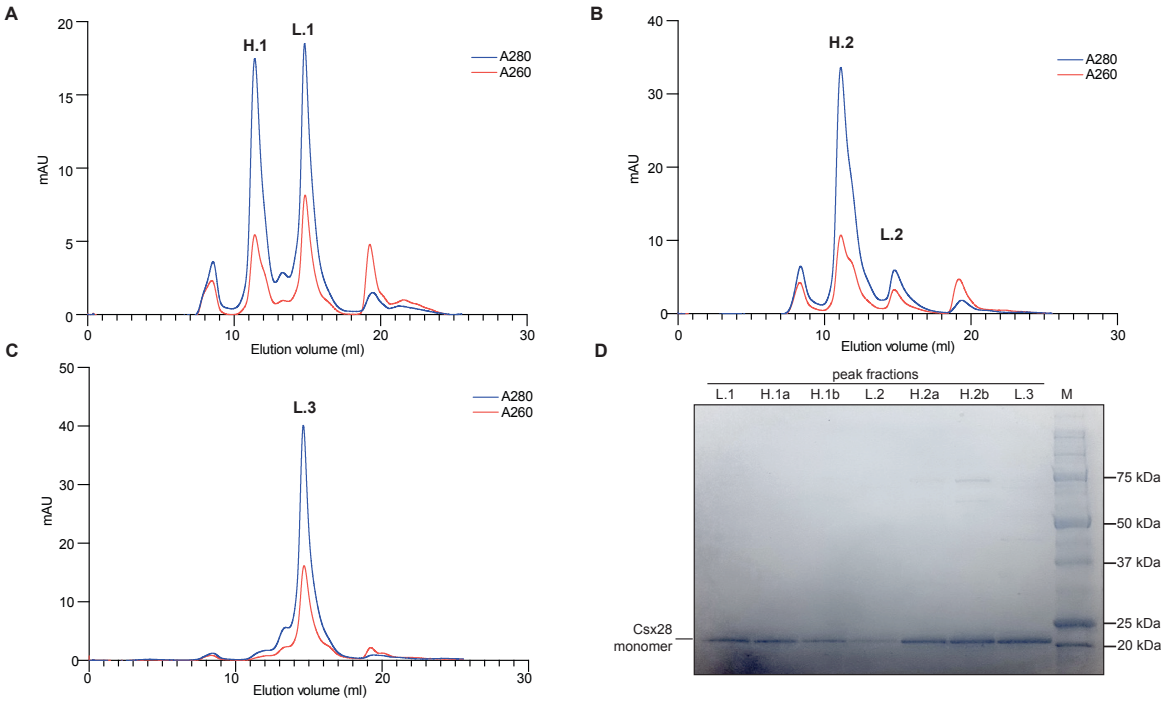


Fig S5. Full length Csx28 can be purified from *E. coli* to homogeneity and exists primarily in two distinct non-exchanging oligomeric states. (**A**) Size exclusion chromatography trace of Csx28. "Light" and "Heavy" peaks are labeled as L.1 and H.1, respectively. These peaks were separately pooled and concentrated, and then subjected to an additional size exclusion cleanup step to generate (**B**) for the Heavy fraction and (**C**) for the Light fraction. The Heavy and residual Light peak in (B) are labeled "H.2" and "L.2", respectively and in (C) the Light peak is labeled L.3. These were all separately pooled and concentrated for subsequent experiments. (**D**) SDS-PAGE analysis of fractions from (A-C). H.1a, H.1b, and H.2a and H.2b were sampled from two separate fractions in the H.1 peak in (A) and H.2 peak in (B), respectively, prior to pooling the fractions.

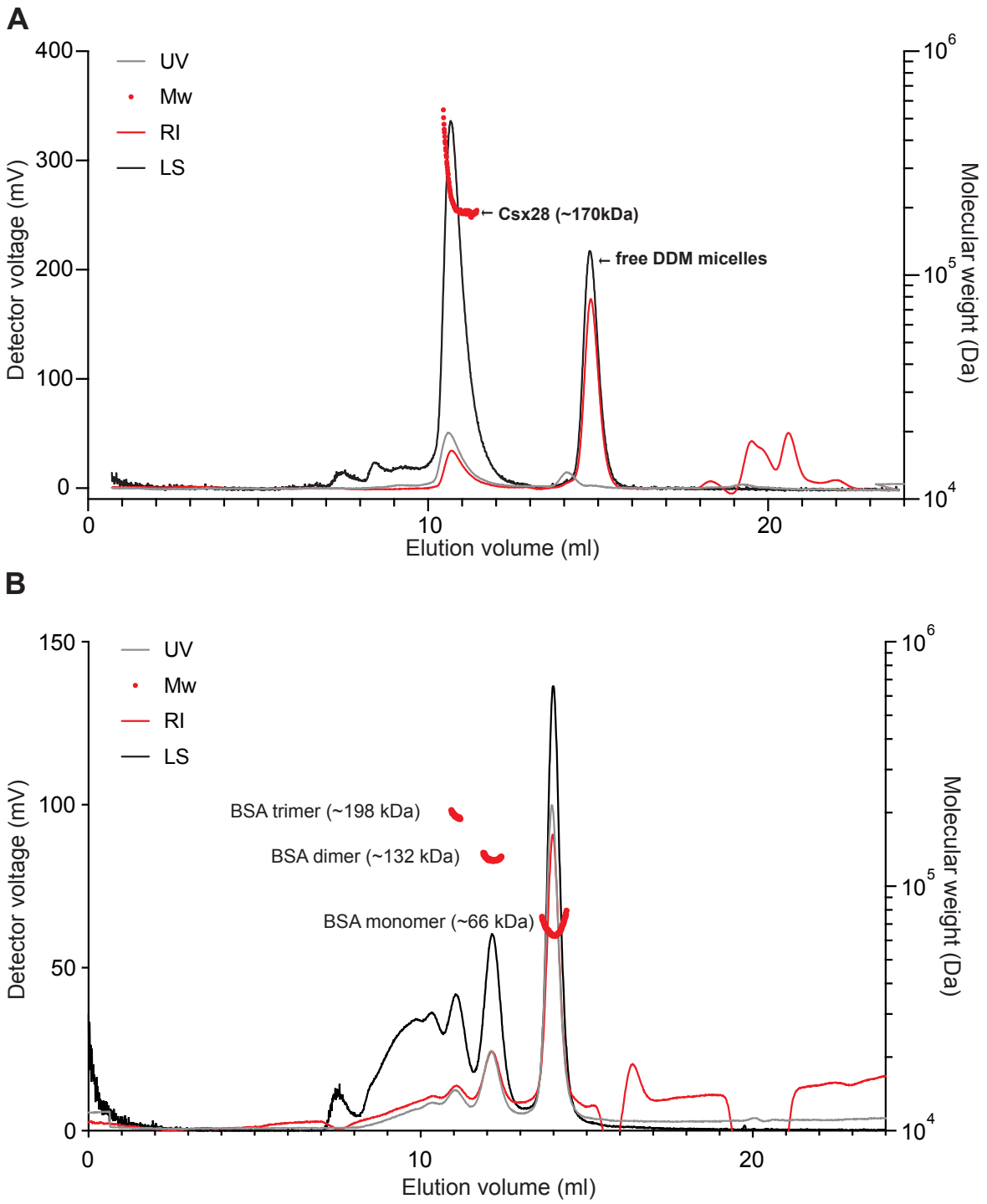


Fig. S6. SLS-SEC reveals that Csx28 forms octamers in solution that are in intermediate exchange with a larger oligomer over the course of the SEC run. Three detector (UV: UV 280 nm absorbance, RI: refractive index, LS: static light scattering) traces for (**A**) Csx28 and (**B**) BSA, as a SLS-SEC sizing control and reference. Molecular weights were determined using the three-detector method (*68*). The experimentally determined molecular weights of each peak are shown.

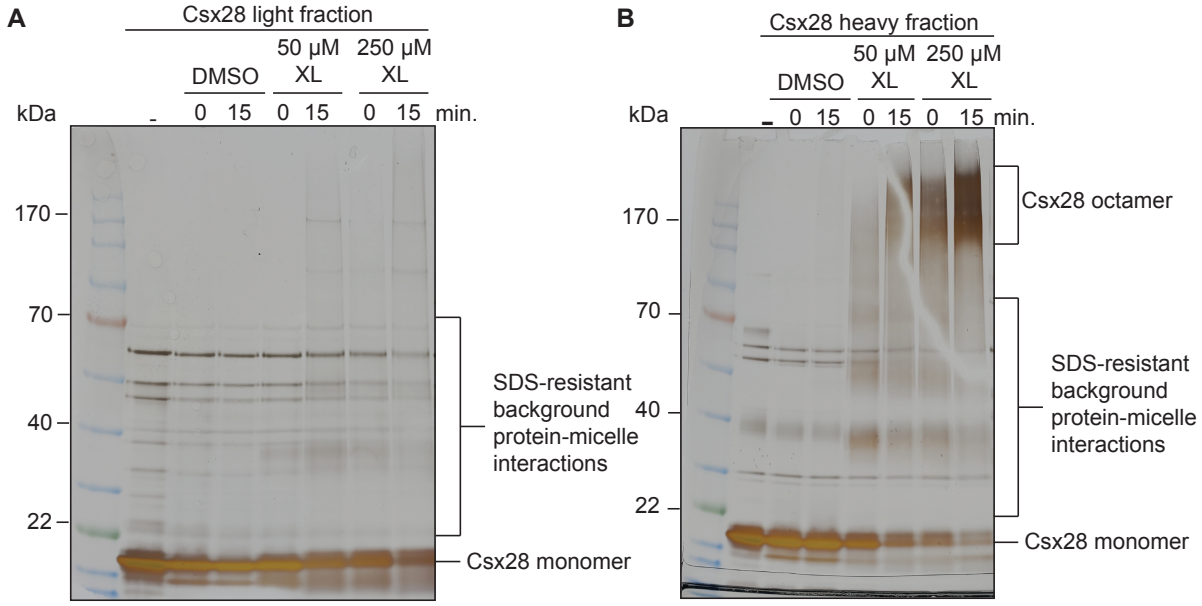


Fig. S7. ***In vitro*** **protein crosslinking with bis[sulfosuccinilimidyl] glutarate-d0 (BS2G-d0) crosslinker reveals that Csx28 (light fraction) is mostly monomeric while Csx28 is mostly octameric in solution. (A)** Silver-stained SDS-PAGE of Csx28 (light fraction) treated with BS2G-d0 crosslinker (5 mM and 25 mM in DMSO) or DMSO (as a vehicle control) for zero or fifteen minutes, using untreated protein as a negative control (~21 kDa). **(B)** Silver stained SDS-PAGE of Csx28 (heavy fraction). treated with BS2G-d0 crosslinker (5 mM and 25 mM in DMSO) or DMSO (as a vehicle control) for zero or fifteen minutes, using untreated protein as a negative control (~21 kDa). In both cases, as indicated, we observe additional faint banding that appears in all samples corresponds to low-levels of SDS-resistant Csx28-micelle interactions. This is a phenomenon well known to occur with helical membrane proteins (*87*) and is detected here due to the sensitive nature of silver-staining.

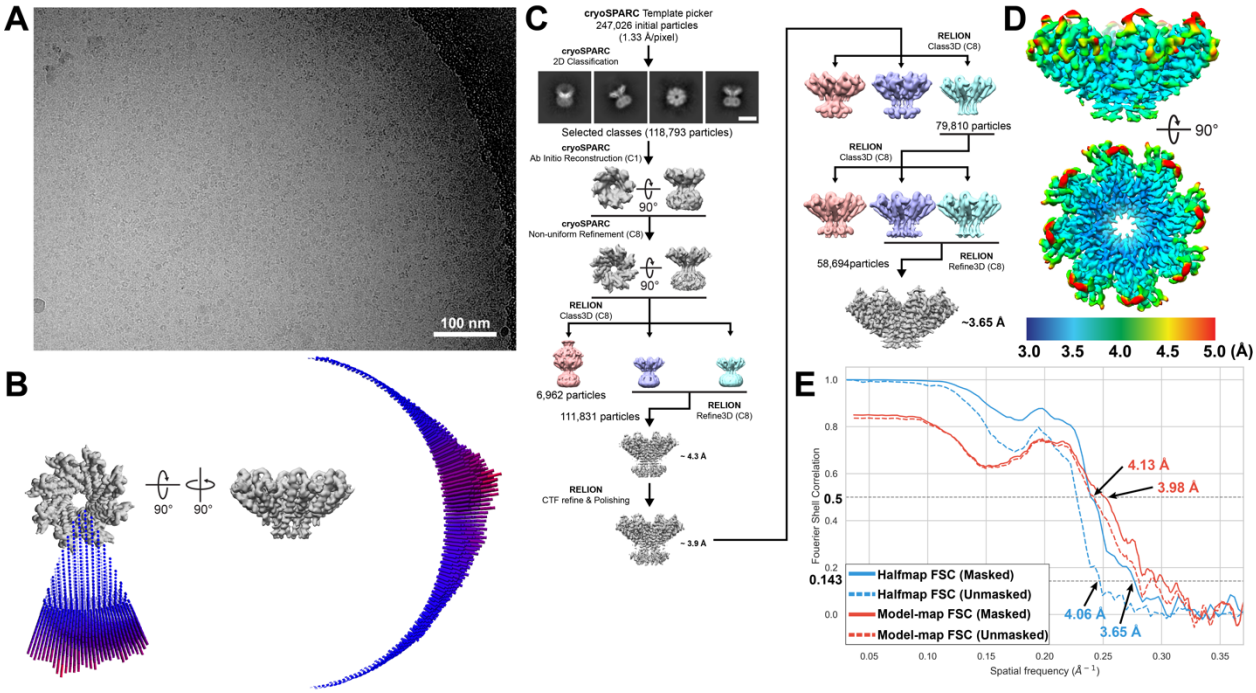


Fig. S8. Cryo-EM data collection and image processing of a Csx28 octamer.
(**A**) Representative micrograph from graphene oxide covered cryo-EM grid of Csx28. Images were taken using Talos Arctica equipped with a K3 direct electron detector. Scale bar represents 100 nm. (**B**)**.** Euler angle orientation distribution of the final reconstruction of Csx28 using C8 symmetry in RELION (*74*). (**C**) Image processing workflow for the Csx28 octamer. Scale bar in 2D class average represents 100 Å. Since 2D average of the top-view, and the initial *ab initio* reconstruction showed clear 8-fold rotational symmetry, C8 symmetry was applied in the following refinements. (**D**) Local resolution of Csx28 octamer is estimated using cryoSPARC (*73*). Legend on the bottom of the panel represents the corresponding resolution for the surface color of the reconstruction. (**E**) Fourier shell correlation (FSC) plot of the Csx28 reconstruction and model. Solid or dashed lines indicate masked or unmasked FSC curves, respectively. FSC between half-maps (blue) or between full-map and atomic model (red) is presented with the estimated resolution using the corresponding cutoff (0.143 for half-maps, 0.5 for model-map FSC).

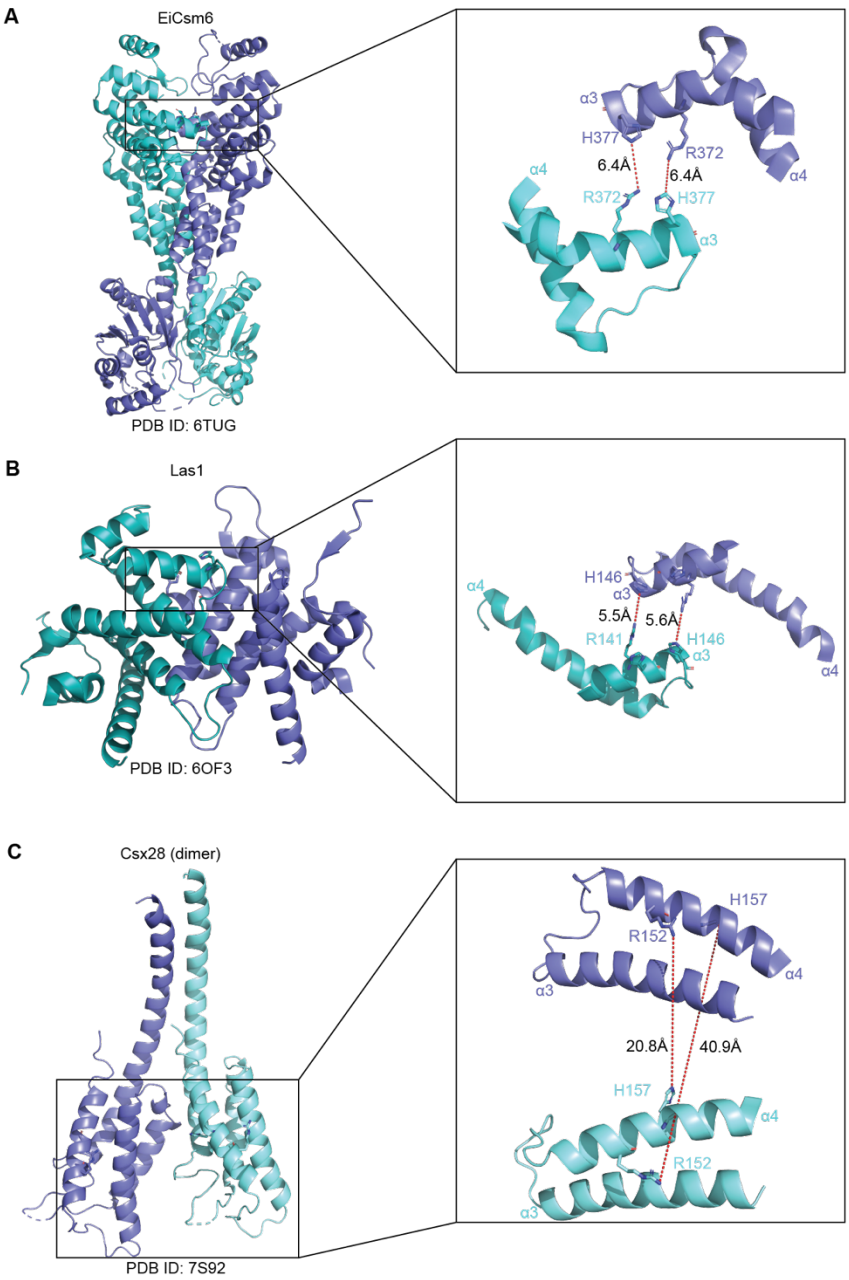


Figure S9. Structural comparison between bona-fide HEPN nuclease proteins Csm6, Las1, and our structure of Csx28 highlights significant differences between interface and residue positioning. A cartoon representation of **(A)** EiCsm6, a cOA-activated HEPN nuclease (*88*) and (**B**) Las1, a part of the RNase complex involved in pre-rRNA processing (*89*). The zoomed-in region shows a closeup of the HEPN active site with the HEPN motif R and H residues shown as stick figures and the distances between the residues shown. (**C**) A cartoon representation of our Csx28 structure (shown as a dimer for brevity). The zoomed-in region shows a closeup of the protomer:protomer interface between Csx28 monomers with the previously predicted "HEPN motif" residues shown as sticks. The very different orientations, helical positions of these residues (α4 in C vs. α3 in A and B), and the significantly larger distances between these residues across the protomer interfaces highlight that Csx28 does not contain a canonical HEPN domain.

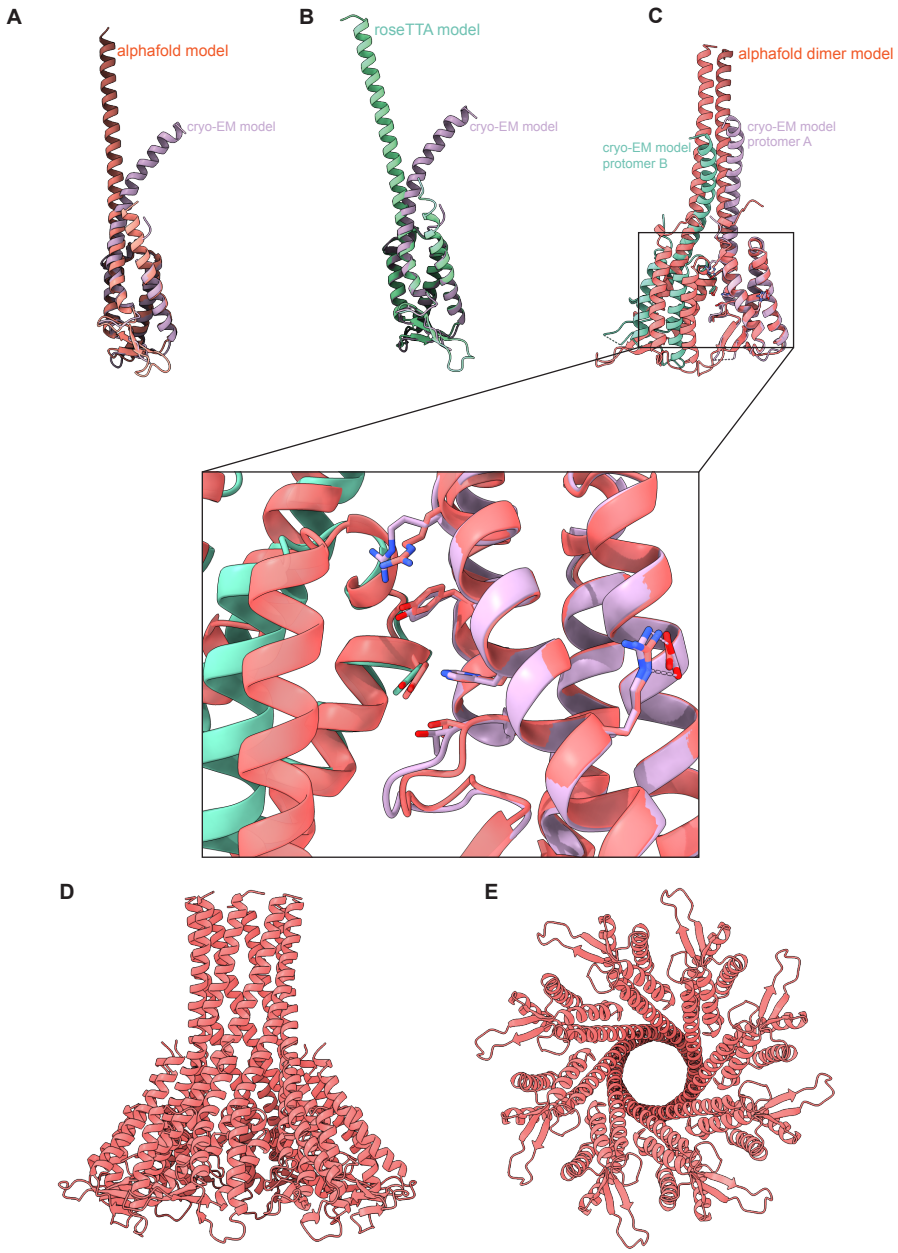


Fig. S10. AlphaFold and RoseTTA predict a highly similar monomeric fold to our Csx28 cryo-EM model and AlphaFold-Multimer predicts a highly similar protomer-protomer interface and homo-octamer of Csx28. (**A**) A structural alignment of Csx28 monomers derived from an AlphaFold prediction and our cryo-EM model. ChimeraX Matchmaker score: 660, RMSD of 88 pruned atom pairs: 0.746 Å, and all pairs (144): 6.876Å. **(B)** A structural alignment of Csx28 monomers derived from a RoseTTA prediction and our cryo-EM model. ChimeraX Matchmaker score: 664.8, RMSD of 88 pruned atom pairs: 1.211 Å, and all pairs (144): 5.851Å. **(C)** A structural alignment of Csx28 dimers derived from an AlphaFold-Multimer prediction and our cryo-EM model. The zoomed-in region shows a protomer:protomer interface with important side chains as sticks. ChimeraX Matchmaker score: 669, RMSD of 102 pruned atom pairs: 0.102 Å, and all pairs (144): 7.880Å. (**D-E**) side and top views, respectively, of an AlphaFold-Multimer prediction of a Csx28 octamer.

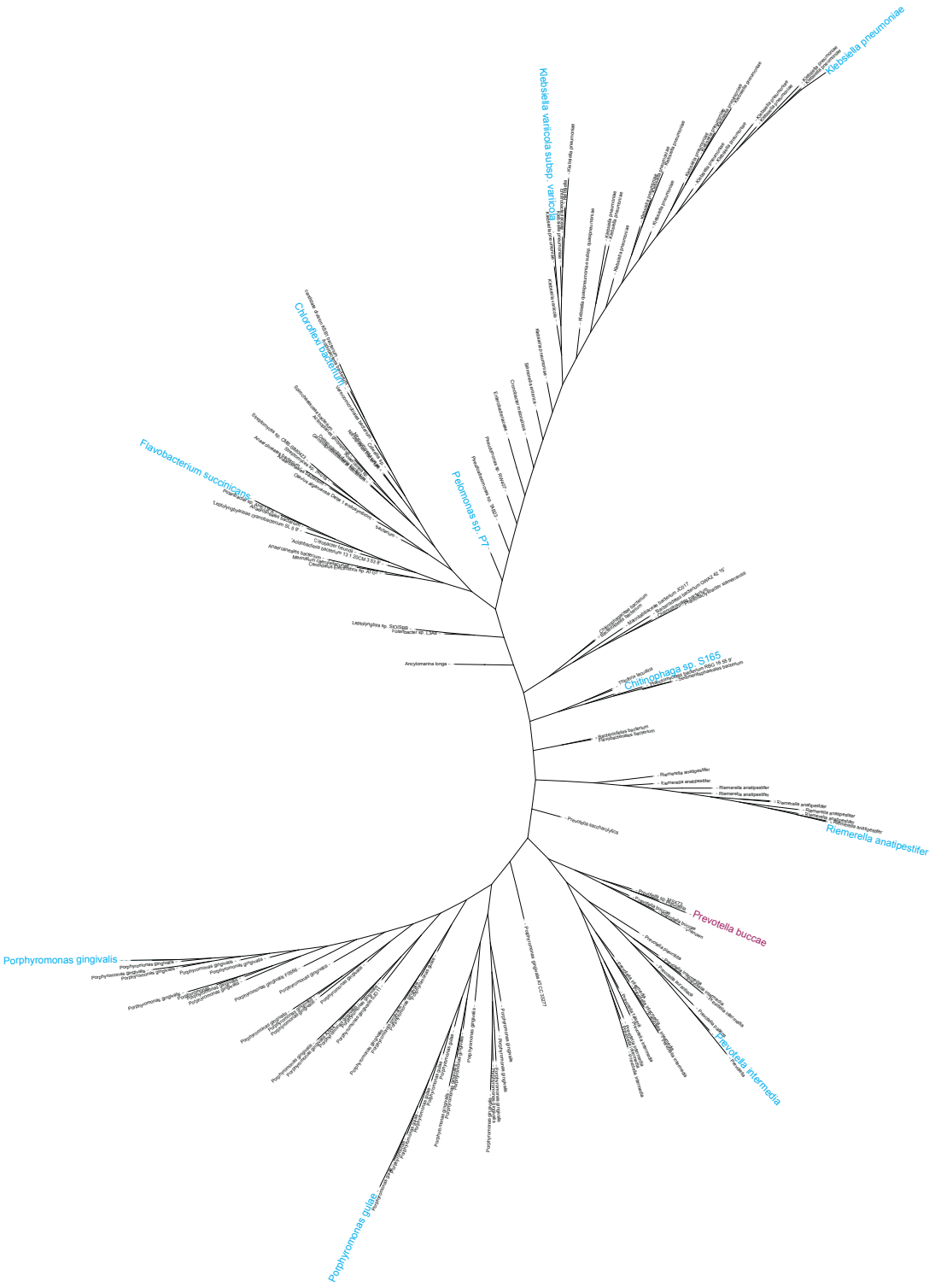


Fig. S11 An unrooted phylogenetic tree of predicted Csx28 orthologs. The top 500 hits from six iterations of PSI-BLAST are shown (see Methods for details). The ten orthologs selected for further DeepTMHMM analysis and AlphaFold-Multimer prediction are shown in light blue, while PbuCsx28 ortholog used in this study is shown in purple. For easier visualization, branch lengths were ignored when constructing this tree for easier visualization.

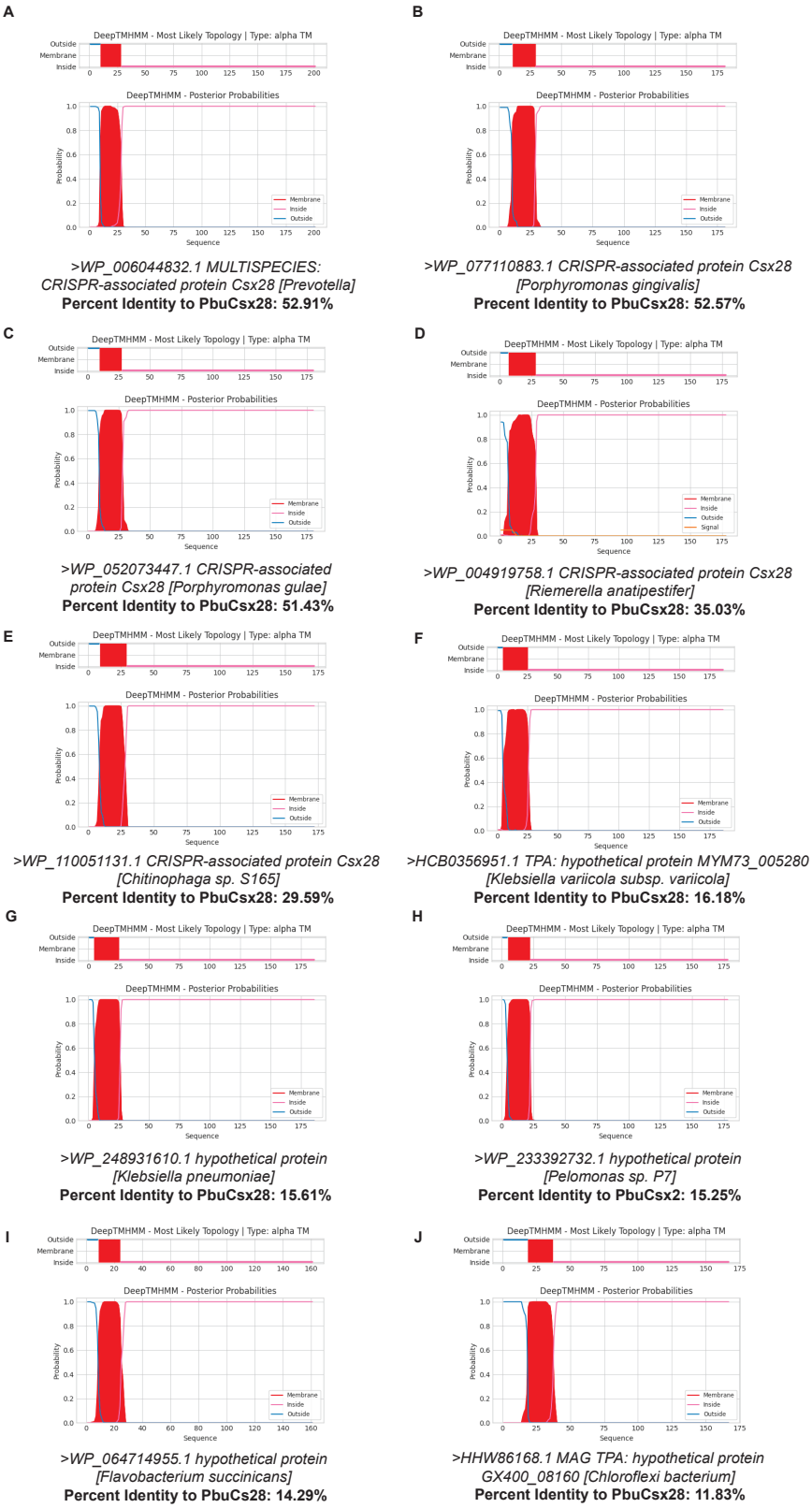


Fig. S12 DeepTMHMM transmembrane-spanning region prediction for the ten Csx28 orthologs selected in Fig S11. Percent sequence identity relative to PbuCsx28 is also indicated and ordered from highest (A) to lowest (J). see Methods for details.

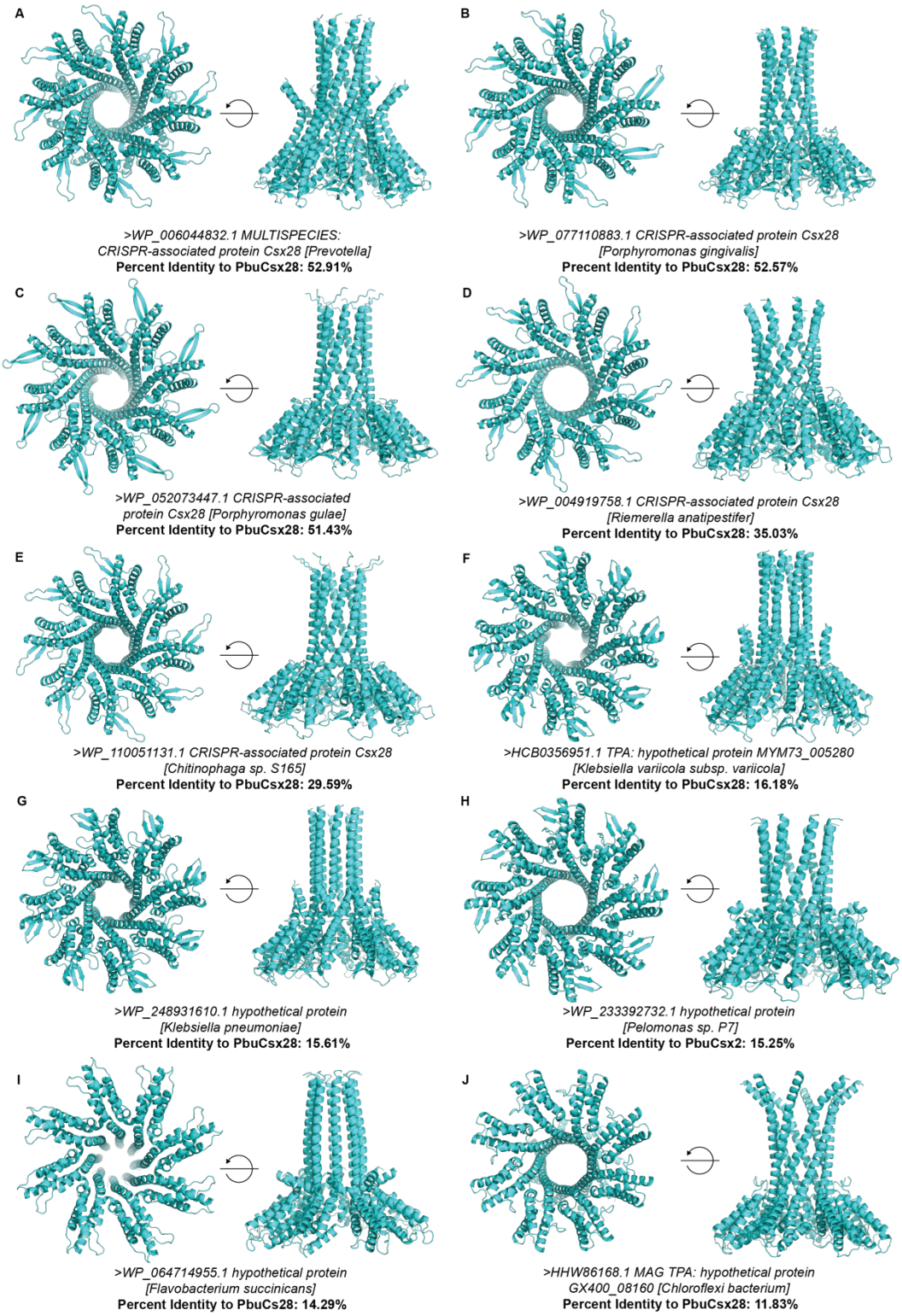


Fig. S13 AlphaFold-Multimer octamer predictions for the ten Csx28 orthologs selected in Fig. S11. Top and side views of highested ranked model in each prediction are shown. Percent sequence identity relative to PbuCsx28 is indicated and ordered from highest (A) to lowest (J). See Methods for details.

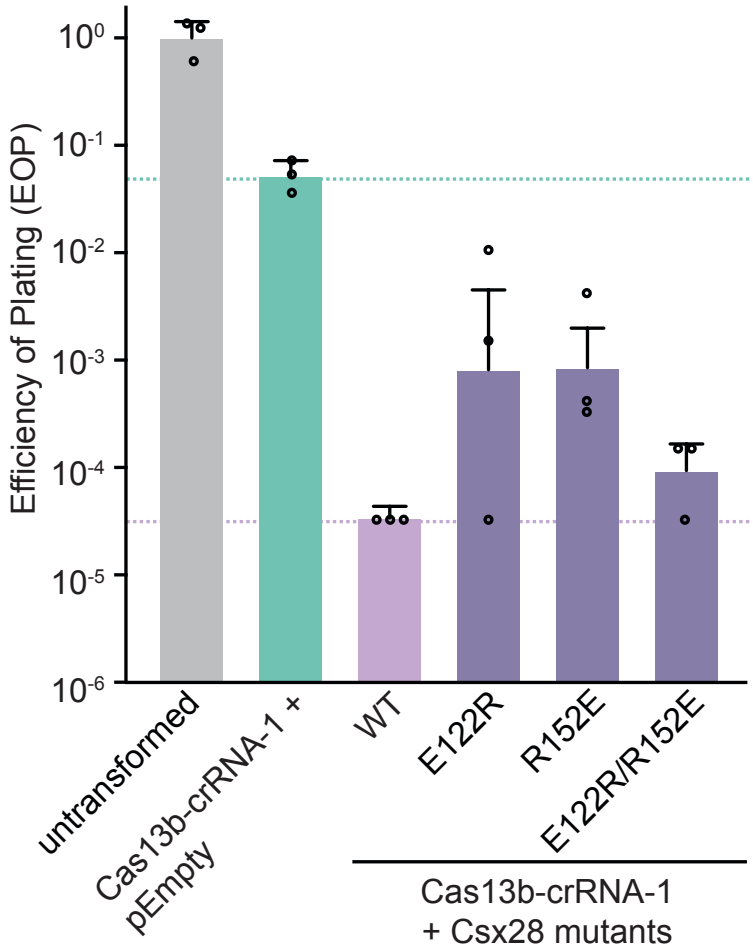


Fig. S14. Charge swap analysis of the potential E122:R152 salt bridge provides further evidence that R152 is engaged in a salt bridge and likely not playing a role in the Csx28 protomer:promoter interface. Efficiency of Plating (EOP) assays measuring λ-phage infection susceptibility of *E. coli* strains carrying the indicated Cas13b-crRNA-1, and WT or mutant Csx28 plasmids. Data is shown as mean ± s.e.m for $n = 3$ biological replicates. For some Cas13b-crRNA-X + pCsx28 samples, an uncountable number of plaques were present in the previous dilution but offered no countable plaques on the subsequent dilution. Therefore, in these cases, the titer is calculated as one plaque for the subsequent dilution.

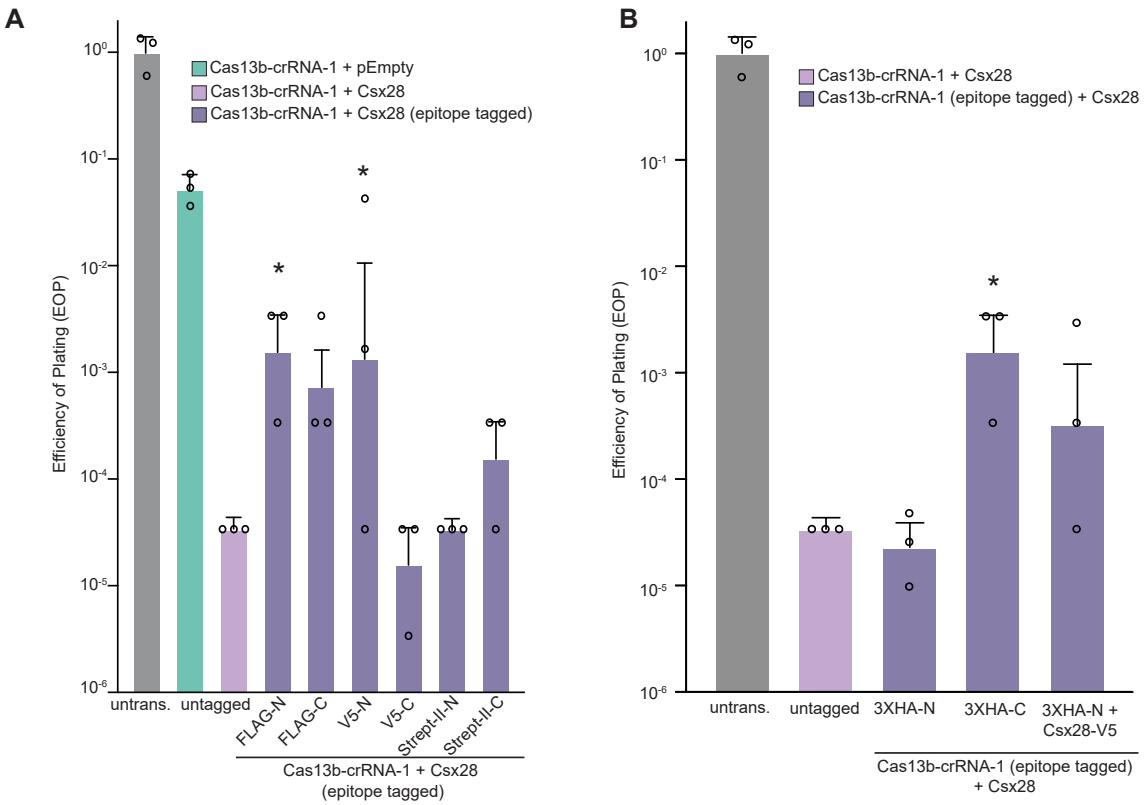


Fig. S15. Cas13b and Csx28 anti-phage defense activity is differentially affected by the choice of epitope tag sequence and location. (**A**) Efficiency of Plating (EOP) assays measuring λ-phage infection susceptibility of untransformed (untrans.) *E. coli* or strains carrying the indicated Cas13b-crRNA-1 and WT or epitope-tagged Csx28 plasmids. (**B**) Efficiency of Plating (EOP) assays measuring λ-phage infection susceptibility of *E. coli* strains carrying the indicated epitope-tagged Cas13b-crRNA-1 and epitope tagged Csx28 plasmids. Data is shown as mean ± s.e.m for $n = 3$ biological replicates. For some Cas13b-crRNA-X + pCsx28 samples, an uncountable number of plaques were present in the previous dilution but offered no countable plaques on the subsequent dilution. Therefore, in these cases, the titer is calculated as one plaque for the subsequent dilution. Statistical significance was calculated using one-way ANOVA and Dunnett's multiple comparisons test, comparing mutant Csx28 strains to wild type Csx28. No significance was detected, unless indicated ($*p \leq 0.05$).

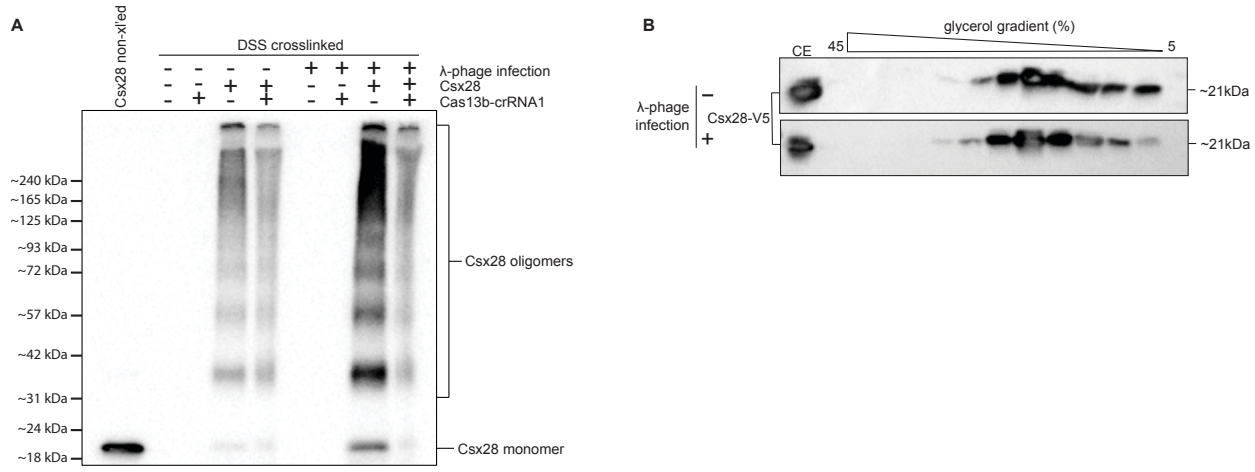


Fig. S16. Csx28 form oligomers *in vivo* independent of λ-phage infection and the oligomeric form doesn't shift during λ-phage infection. (**A**) A Western blot detecting qualitative Csx28 crosslinking *in vivo*. Cas13b-crRNA-1 and V5-tagged Csx28 expressing *E. coli* in the absence or presence of λ-phage infection (MOI: 0.1) were harvested 1 hour post-infection, subjected to DSS crosslinking in culture, subsequently lysed and total cell lysates were subjected to SDS-PAGE prior to Western blot analyzes. A non-crosslinked Csx28-expressing total cell lysate (Csx28 non-xl'ed) was used as a control. The presence of multiple, heterogenous oligomeric forms and smearing is likely due to inefficient and heterogeneous Csx28 protomer:protomer crosslinking that is known to occur when using this crosslinker *in vivo*, as well as differential SDS binding due to crosslinking modifying the chemical status of the polypeptide. As a result, we cannot make quantitative conclusions about oligomeric dynamics and distributions based on this experiment alone. (**B**) A Western blot detecting Csx28's position in a 5-45% glycerol gradient post ultracentrifugation in the absence or presence of λ-phage infection. Cas13b-crRNA-1 and V5-tagged Csx28 expressing *E. coli* C3000 strains were infected with λ-phage (MOI: 0.1) and then harvested 90 min. post infection CE: cell extract prior to fractionation. No change in the position of Csx28 pre- and post- λ-phage infection indicates there is no large changes in oligomerization dynamics in the absence or presence of phage λ-phage infection. All blots were probed with an anti-V5 antibody to detect Csx28-V5.

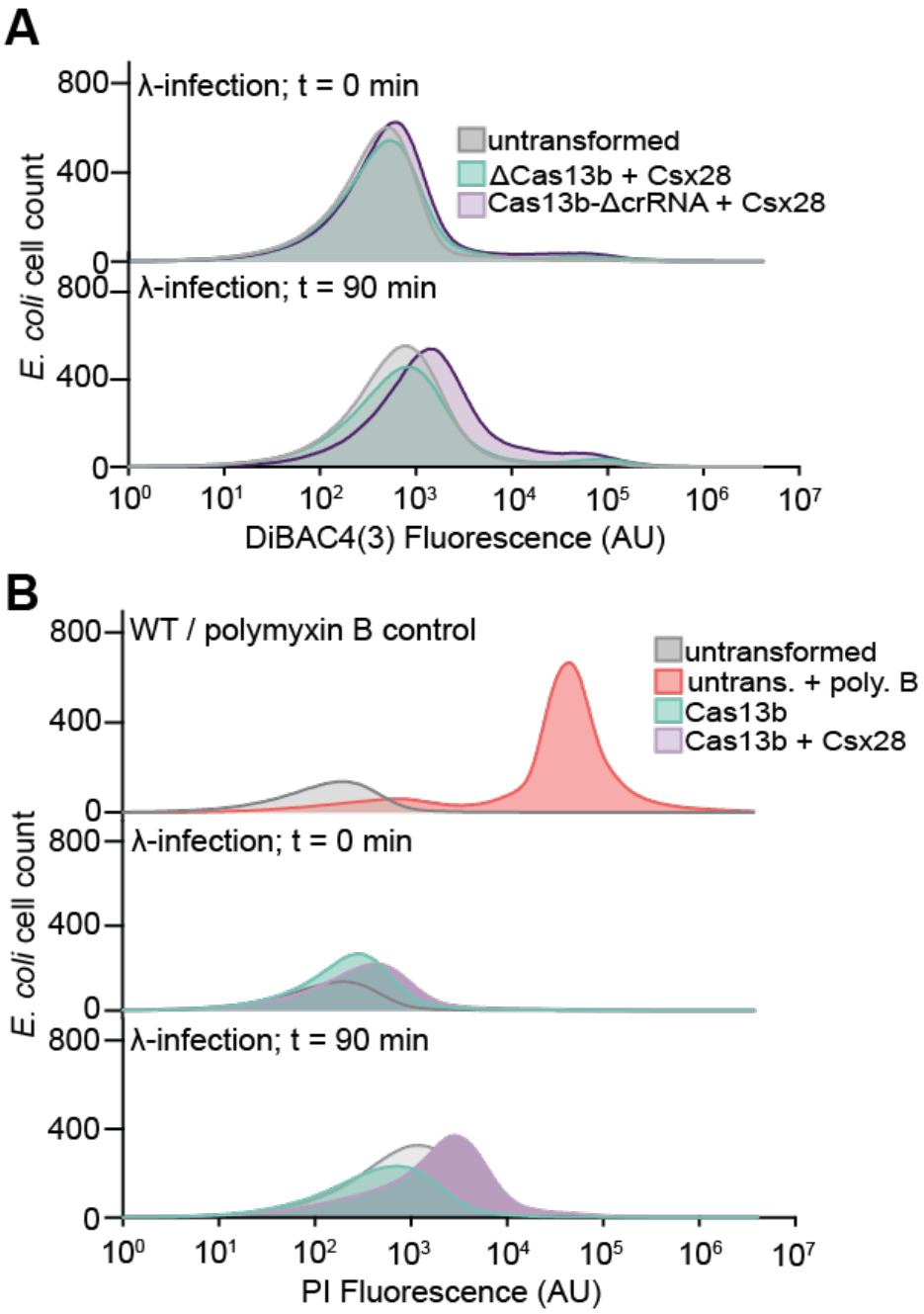


Fig. S17. Csx28 expression alone cannot induce membrane depolarization and Csx28 activation doesn't lead to a substantial uptake of propidium iodide. (**A**) Flow cytometry histograms of a DiBAC4(3) staining assay measuring membrane depolarization of untransformed *E. coli or E. coli* strains expressing Cas13b-crRNA-1 and Csx28, or Cas13b-ΔcrRNA and Csx28 over the course of a λ-phage infection (MOI of 1). (**B**) Flow cytometry histograms of a propidium iodide (PI) staining assay measuring gross membrane integrity of untransformed (untrans.) *E. coli or E. coli* strains expressing Cas13b-crRNA-1, or Cas13b-crRNA-1 and Csx28 over the course of a λ-phage infection (MOI of 1). A Polymyxin B (Poly. B; a membrane integrity disrupter) treated *E. coli* sample was used as positive control for loss of membrane integrity. In all samples above, 10,000 *E. coli* cells were analyzed.

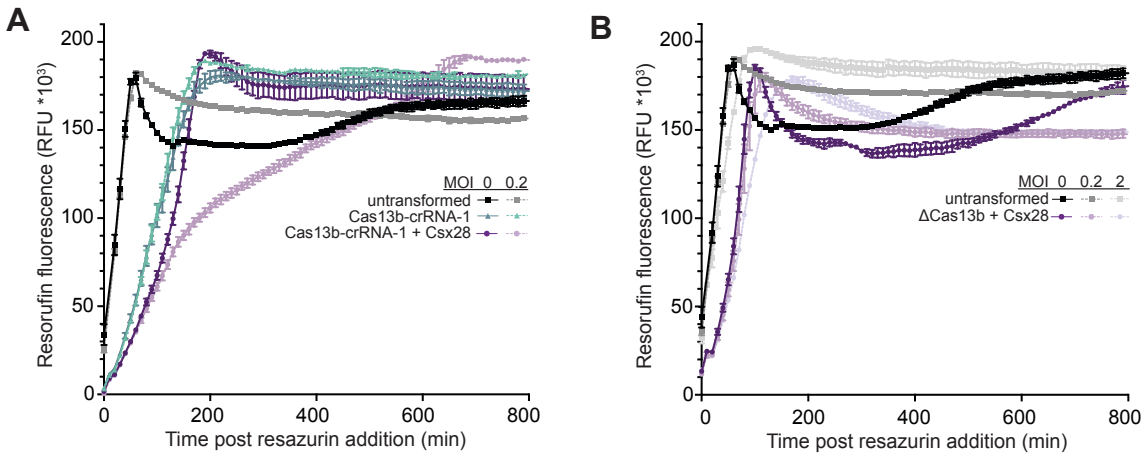


Fig. S18. Activated Csx28 results in loss of metabolic activity at low MOI infection and requires Cas13b-mediated activation for this effect. Resazurin metabolism assay measuring the conversion of resazurin to fluorescent resorufin over time as a function of active respiration for (A) untransformed *E. coli or E. coli* strains expressing Cas13b-crRNA-1, or Cas13b-crRNA-1 and Csx28 either in the absence or presence of λ-phage infection (MOI of 0.2), or (B) untransformed *E. coli or E. coli* strains expressing Cas13b-crRNA-1 and Csx28 either in the absence or presence of λ-phage infection (MOI of 0.2 and 2). Resazurin is added to the growing cultures at one hour post λ-phage infection. Data is shown as mean ± s.e.m for $n = 3$ biological replicates.

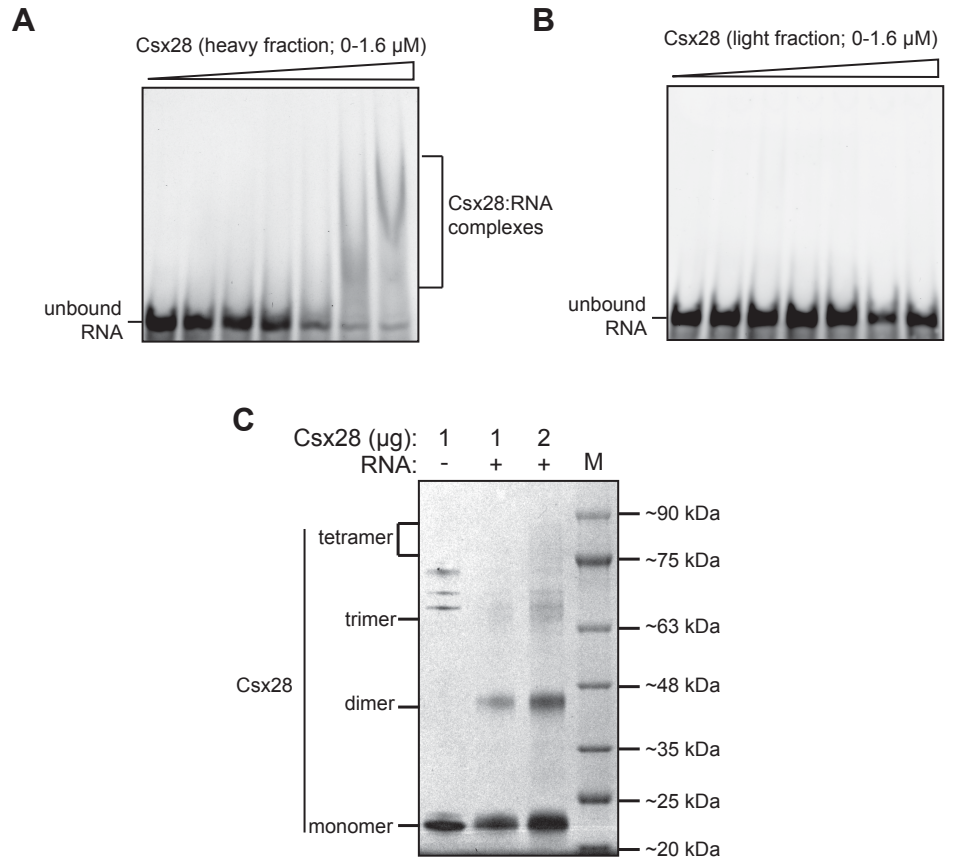


Fig. S19. Csx28 binds and crosslinks to RNA *in vitro.* Electrophoretic Mobility Shift Assays (EMSAs) for binding reactions between (A) Octameric (heavy fraction) Csx28 or (B) monomeric (light fraction) Csx28 and a short fluorescently-labeled RNA oligonucleotide. In both cases [RNA] was held constant at 100 nM and [Csx28] was titrated from 0-1.6 μM, incubated at 37ºC for 1h and visualized using 8% native PAGE. (C) SDS-PAGE of Csx28 (heavy fraction) in absence or presence of a short RNA oligonucleotide post UV crosslinking, as indicated. Assembled complexes were then UV-irradiated in quartz cuvettes using UV Stratalinker 1800 (wavelength 254 nm) at 120,000 microjoules/cm^2. The Csx28 cross-linked products were denatured in SDS-loading buffer at 95 °C for 10 minutes, loaded onto Bis-Tris 4-12% gradient gel, followed by sample separation at 150 V for 90 minutes and gel staining with silver stain.

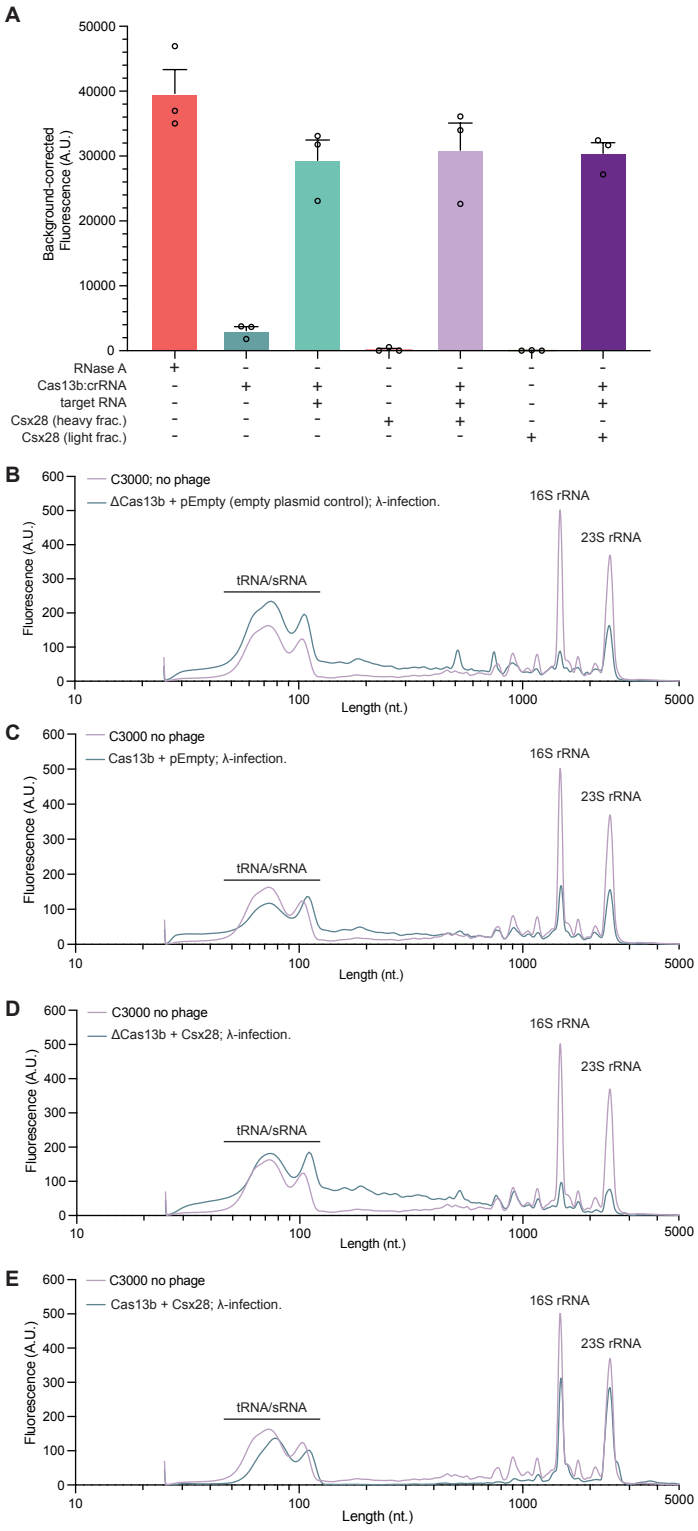


Fig. S20. Purified PbuCas13b possesses robust collateral RNA cleavage *in vitro* that is not enhanced in the presence of Csx28, and detection of Cas13b-mediated collateral cleavage *in vivo* is complicated due to the large changes in RNA abundance distributions upon λ-phage infection (**A**) Background-corrected fluorescence values from an *in vitro* collateral cleavage assay testing the ability for Cas13b to cleave a fluorescent ssRNA reporter in *trans* in the

absence or presence of Csx28 as indicated. An RNase A treated sample is shown as a positive RNA degradation control (mean ± s.e.m, n = 3). AU: arbitrary units. (**B-E**) Bioanalyzer traces of total RNA extracted from the indicated strains in the absence or presence of a λ-phage infection (MOI of 0.2). RNA was extracted 90 minutes post infection and loaded onto an Total RNA 6000 Pico Chip and analyzed via capillary electrophoresis on a Bioanalyzer 2100 Instrument. rRNA and tRNA/sRNA regions are indicated.

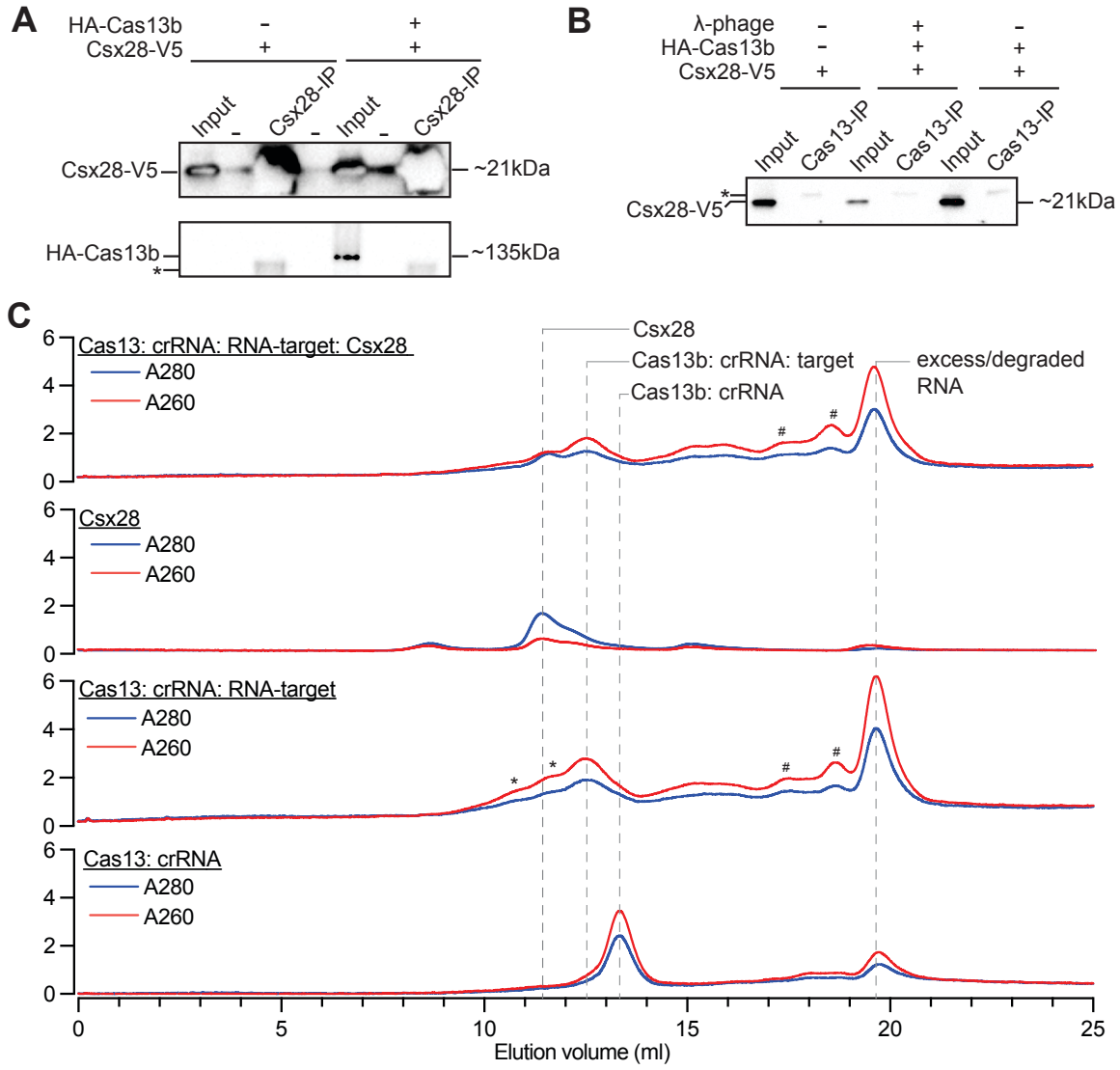


Fig. S21. A direct interaction between target-RNA bound Cas13b:crRNA and Csx28 isn't observed using either co-immunoprecipitations from *in vivo* λ-phage infection assays or analytical size-exclusion experiments using purified Cas13:crRNA:target-RNA in the absence or presence of Csx28. (**A**) A Western blot of a Csx28-V5 immunoprecipitation in the absence or presence of HA-Cas13b during λ-phage infection (MOI: 0.1). HA-tagged Cas13b-crRNA-1 and V5-tagged Csx28 expressing *E. coli* subject to λ-phage infection were subsequently lysed and total cell lysates (solubilized with Triton-X100) were subjected to an anti-V5 immunoprecipitation, SDS-PAGE and Western blot analyzes. Blots were first probed with an anti-V5 antibody to detect Csx28-V5 followed by anti-HA antibody to detect HA-Cas13b. The band indicated by an asterisk (*) is a background interaction between the secondary antibodies and leached primary antibody from the IP beads and doesn't correspond to HA-Cas13b. It should be noted that the samples were purposefully overloaded (with respect to Csx28-V5 blotting) to provide the best opportunity to observe any potential interaction with HA-Cas13b, however none was detected. (**B**) A western blot of a HA-Cas13b immunoprecipitation in the presence of Csx28-V5 and in the absence or presence of λ-phage infection (MOI: 0.1). HA-tagged Cas13b-crRNA-1 and V5-tagged Csx28 expressing *E. coli* subject to λ-phage infection

(as indicated) were subsequently lysed, membrane fractionated, and the inner membrane fraction was subjected to an anti-HA immunoprecipitation, SDS-PAGE and Western blot analyzes. Blots were probed with an anti-V5 antibody to detect Csx28-V5. The band indicated by an asterisk The band indicated by an asterisk (*) is a background interaction between the secondary antibodies and leached primary antibody from the IP beads and doesn't correspond to HA-Cas13b and doesn't correspond to Csx28-V5, and thus no interaction was detected here. (**C**) Analytical size-exclusion chromatography of purified and active Cas13b:crRNA or Csx28 in the absence or presence of an RNA-target and/or Csx28, as indicated. The indicated samples were incubated for 30 minutes at 37ºC prior to being loaded onto a Superdex 200 increase column running at 0.5 ml/min at 4ºC. The identity of each peak is indicated. Peaks marked with # correspond to degraded RNA peaks (from Cas13b:crRNA activity on the target RNA), while peaks marked with * correspond to various minor forms of Cas13:crRNA:RNA-target (possibly complexes containing target-RNA that is still bound but partially cleaved). If a Cas13b:crRNA:target-RNA complex including Csx28 existed, we would expect an additional earlier eluting peak to be observed, however, no such peak is detected (top trace). Absence of this additional peak suggests, in the given conditions, that target bound Cas13b does not form a stable physical interaction with octameric Csx28. In addition, we do not see the appearance of a Csx28 monomer peak in the top trace, suggesting that under these conditions a Cas13b:crRNA:target-RNA complex is not able to dissemble the Csx28 octamer, thus ruling out an octamer->monomer transition as a potential mechanism of action.

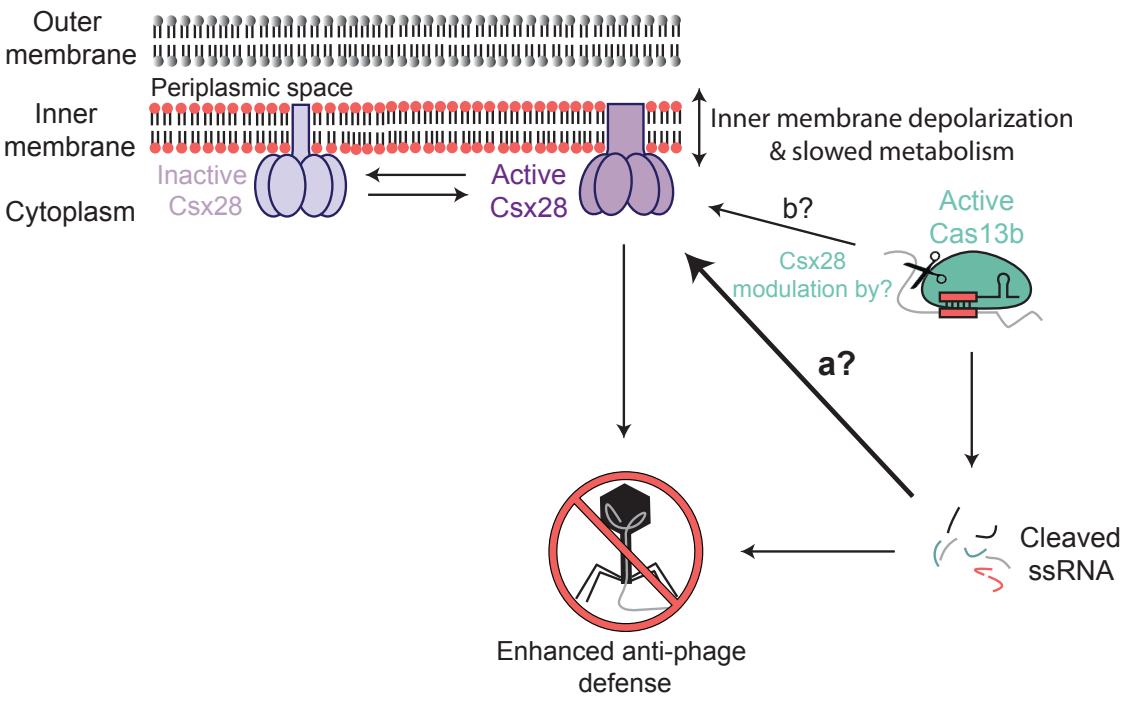


Fig. S22. A hypothetical model for Cas13b-dependent Csx28-mediated anti-phage defense. A hypothetical model describing Csx28's role in enhancing TypeVI-B2 anti-phage defense. Csx28 resides in the membrane prior to phage infection and exists in an inactive state, whereas Cas13b:crRNA complexes reside in the cytoplasm. Upon successful detection of phage transcripts by Cas13:crRNA complexes, Cas13's HEPN nuclease is activated for ssRNA cleavage, which results in RNA degradation of both viral and host transcripts. We hypothesize subsequent Csx28-mediated membrane depolarization is likely modulated via (a) activation of Csx28 function through an interaction with Cas13-generated RNA cleavage products, which possess non canonical RNA termini (5' hydroxyls and 3'cyclic phosphates) that may act as a specific signal for Csx28 activation or less likely via (b) a direct binding interaction between Csx28 and HEPN-activated Cas13:crRNA:target-RNA. We can also not discount Cas13 signaling indirectly to Csx28 through yet to be determined factors.

Table S1. Cryo-EM Statistics for Data Collection and Model Refinement.

Name	Csx28 octamer
PDB ID	8GI1
EMDB ID	EMD-40059
Data collection and Processing	
Microscope	Talos-Arctica
Voltage (keV)	200
Camera	K3
Magnification	63,000
Pixel size at detector (Å/pixel)	1.33
Total electron exposure (e^{-}/Å^2)	47
Exposure rate (e-/pixel/sec)	28.09
Number of frames collected during exposure	44
Defocus range (mm)	-1 – -2.5
Automation software	SerialEM
Energy filter slit width	20 keV
Micrographs collected (no.)	904
Micrographs used (no.)	314
Total extracted particles (no.)	247,026
For each reconstruction:	
Refined particles (no.)	118,793
Final particles (no.)	58,694
Symmetry	C8
Resolution (global, Å)	
FSC 0.5 (unmasked/masked)	4.43/4.18
FSC 0.143 (unmasked/masked)	4.06/3.65
Resolution range (local, Å)	3.5 – 5
Resolution range due to anisotropy (Å)	3.5 – 3.8
Map sharpening *B* factor (Å^2)	-118
Map sharpening methods	RELION
Model composition	
Protein residues	1,152
Ligands	0
RNA/DNA	0
Model Refinement	
Refinement package	Coot/Rosetta
- real or reciprocal space	Real
- resolution cutoff (Å)	3.5
Model-Map scores	

- CC	0.79
- Average FSC (0.5 cutoff, Å)	3.98
R.m.s deviations from ideal values	
Bond length (Å)	0.017
Bond angles (°)	1.483
Validation	
MolProbity score	1.80
CaBLAM outliers (%)	4.07
Clashscore	9.89
Poor rotamers (%)	0
C-beta outliers (%)	1.06
EMRinger score	2.14
Ramachandran plot	
Favored (%)	95.9
Outliers (%)	0.0

Table S2. Plasmids used in this study.

Plasmid	Description	Source
pPbuCas13b-cRNA-X	Lac inducible promoter modification of Addgene #89906 (Cam^R)	This study
pPbuCas13b-ΔcrRNA	Deletion of crRNA and promoter region	This study
pPbuCas13b-crRNA1	Spacer targeting λ N gene	This study
pPbuCas13b^{dHEPN}-crRNA1	Deactivated nuclease activity of HEPN (R156A/H161A/H1073A/R1068A)	This study
pPbuCas13b-crRNA2	Spacer targeting λ Q gene	This study
pPbuCas13b-crRNA3	Spacer targeting λ R gene	This study
pPbuCas13b-crRNA-MS2	Spacer targeting MS2 replicase gene	This study
pΔPbuCas13b	Deletion of Cas13b orf	This study
pHA-PbuCas13b-crRNA1	N-terminal HA tag	This study
pPbuCas13b-crRNA1-HA	C-terminal HA tag	This study
pPbuCsx28	Lac inducible promoter modification of Addgene #89909 (Amp^R)	This study
pEmpty	Deletion of Csx28 orf and promoter region	This study
pPbuCsx28-Y55A	Conserved structure-guided mutant Y55A	This study
pPbuCsx28-T62A	Conserved structure-guided mutant T62A	This study
pPbuCsx28-Y104A	Conserved structure-guided mutant Y104A	This study
pPbuCsx28-Y104F	Conserved structure-guided mutant Y104F	This study
pPbuCsx28-E122R	Structure-guided mutant E122R	This study
pPbuCsx28-R152A	Predicted HEPN residue mutant R152A	This study
pPbuCsx28-R152E	Structure-guided mutant R152E	This study
pPbuCsx28-H157A	Predicted HEPN residue mutant H157A	This study
pPbuCsx28-R165A	Structure-guided mutant R165A	This study
pPbuCsx28-R165E	Structure-guided mutant R165E	This study
pPbuCsx28-Y104A/H157A	Y104A & H157A double mutant	This study
pPbuCsx28-Y104A/R165A	Y104A & R165A double mutant	This study
pPbuCsx28-R152A/H157A	R152A & H157A double mutant	This study
pPbuCsx28-H157A/R165A	H157A & R165A double mutant	This study
pFlag-PbuCsx28	N-terminal Flag tag	This study
pPbuCsx28-Flag	C-terminal Flag tag	This study
pStrepII-PbuCsx28	N-terminal Strep II tag	This study
pPbuCsx28-StrepII	C-terminal Strep II tag	This study
pV5-PbuCsx28	N-terminal V5 tag	This study
pPbuCsx28-V5	C-terminal V5 tag	This study
p2CcT-PbuCsx28	PbuCsx28-MBP-His_6 overexpression (Amp^R)	This study
p2CT-PbuCas13b	His_6-MBP-PbuCas13b overexpression (Amp^R)	This study

Table S3. Oligonucleotide primers/gene fragments used in this study.

Primer	Sequence
PbuCsx28_Lac Fix_F	atggattatatggaattagcgaaagaggcat
PbuCsx28_Lac Fix_R	agctgtttcctgtgtgaaattgttatcc
Lac sequence_F	acgatataagttgtaattctcatgtgcaattaatgtgagttagctcactcattagg
Lac sequence_R	caaataatttatcttgtttttgcatagctgtttcctgtgtgaaattgt
PbuCas13b_Lac Fix_F	atgcaaaaacaagataaattatttgtagatagaaagaaaaatgct
PbuCas13b_Lac Fix_R	acatgagaattacaacttatatcgtatggggc
λ crRNA-1_F	acaacagctaatccggaatcgcacttacggccaa
λ crRNA-1_R	caacttggccgtaagtgcgattccggattagctg
λ crRNA-2_F	acaaggaaagagagtcagaagccgtggcccgtgg
λ crRNA-2_R	caacccacgggccacggcttctgactctctttcc
λ crRNA-3_F	acaaagatattgctgcaacggtcgattgcctgac
λ crRNA-3_R	caacgtcaggcaatcgaccgttgcagcaatatct
MS2 crRNA-1_F	acaacgagagaaagatcgcgaggaagatcaatac
MS2 crRNA-1_R	caacgtattgatcttcctcgcgatctttctctcg
PbuCsx28_ ΔcrRNA _F	atcgtccattccgacagc
PbuCsx28_ ΔcrRNA _R	ttagtttttattttctgatttttcaatttctttttatggc
ΔPbuCas13b_F	attgacagctagctcagtccta
ΔPbuCas13b_R	acatgagaattacaacttatatcgtatggggc
dPbuCas13b_F1 (R156A/H161A)	tattctgaagaatccccaaaaccgatatttgaaacaagcc
dPbuCas13b_R1 (R156A/H161A)	cttgtacgcggagtagtagttcgcgagaacctgaag
dPbuCas13b_F2 (R1068A/H1073A)	tatcccatgtatgatgccacactctttgctgaagt
dPbuCas13b_R2 (R1068A/H1073A)	ctggttcgcggaaaaagcattcgccactgcaatc
ΔPbuCsx28_F	ccgggtaccgagctcgaattc
ΔPbuCsx28_R	gcgttgcgctcactgccc
PbuCsx28_Y55A_F	aagacagcatattgatttgggaaaaaacaaaagatggtaagc
PbuCsx28_Y55A_R	cattttcagtatttgtagtaaatctgagtagtttcgccaggc
PbuCsx28_T62A_F	aagacagcatattgatttgggaaaaaacaaaagatggtaagc
PbuCsx28_T62A_R	cattttcagtattcgcagtaaatctgagtagtttatacaggc
PbuCsx28_Y104A_F	gatgtggtatttttatgtcaaaagaggctctgtcactaatttcc
PbuCsx28_Y104A_R	cttcgttcgctatttctttggaaagctcttttataaatttgcg
PbuCsx28_Y104F_F	gatgtggtatttttatgtcaaaagaggctctgtcactaatttcc
PbuCsx28_Y104F_R	cttcgttaaatatttctttggaaagctcttttataaatttgcg
PbuCsx28_E122R_F	gtttcatgctttccgcccaaaacaatcc
PbuCsx28_E122R_R	cataaacaatatttctatagcgggaaattagtgacagagcctc
PbuCsx28_R152A_F	tcgatagaaatcagacaagcaatcaatctgaaaaaacgag
PbuCsx28_R152A_R	gaggttttggtgaatctttttcatcgcttctacagactc
PbuCsx28_R152E_F	tcgatagaaatcagacaagcaatcaatctgaaaaaacgag
PbuCsx28_R152E_R	gaggttttggtgaatctttttcatttcttctacagactc
PbuCsx28_H157A_F	tcgatagaaatcagacaagcaatcaatctgaaaaaacgag
PbuCsx28_H157A_R	gaggttttgcgcaatctttttcattcgttctacagactc
PbuCsx28_R165A_F	aatctgaaaaaacgagatttaagattttaaccgggtaccg
PbuCsx28_R165A_R	gattgcttgcgcgatttctatcgagaggttttgg

PbuCsx28_R165E_F	aatctgaaaaaacgagatttaagattttaaccgggtaccg
PbuCsx28_R165E_R	gattgcttgttcgatttctatcgagaggttttgg
1x_Flag_PbuCsx28_F	acaaaggctcttctggttcggattatatggaattagcgaaagaggc
1x_Flag_PbuCsx28_R	cgtcgtcgtccttgtagtccatagctgtttcctgtgtgaaattg
PbuCsx28_1x_Flag_F	caaggacgacgacgacaaataaccgggtaccgagct
PbuCsx28_1x_Flag_R	tagtccgaaccagaagagccaaatcttaaatctcgtttttttcagattg
StrepII_PbuCsx28_F	ggtgggggctcttctggttcggattatatggaattagcgaaagaggc
StrepII_PbuCsx28_R	cggttgaggatgtgcccacgccatagctgtttcctgtgtgaaattg
PbuCsx28_StrepII_F	gcacatcctcaaccgggtgggtaaccgggtaccgagct
PbuCsx28_StrepII_R	ccacgccgaaccagaagagccaaatcttaaatctcgtttttttcagattg
V5_PbuCsx28_F	gtctcgattctacgggctcttctggttcggattatatggaattagcgaaagaggc
V5_PbuCsx28_R	cgaggagagggttagggataggcttacccatagctgtttcctgtgtgaaattg
PbuCsx28_V5_F	taaccctctcctcggtctcgattctacgtaaccgggtaccgagct
PbuCsx28_V5_R	gggataggcttacccgaaccagaagagccaaatcttaaatctcgtttttttcagattg
3x_HA_PbuCas13b_F	cgcatacccgtatgacgttccggactatgccgggtcaagtggctctcaaaaacaagataaattat ttgtagatagaaagaaaaatg
3x_HA_PbuCas13b_R	tagtctggaacgtcgtatggataagcgtagtcagggacatcataagggtacatagctgtttcctgt gtgaaattg
PbuCas13b_3x_HA_F	cgacgttccagactacgcatacccgtatgacgttccggactatgcctaaattgacagctagctca gtcc
PbuCas13b_3x_HA_R	tatggataagcgtagtcagggacatcataagggtaagagccacttgacccgtttttatttttctgatt tttcaatttcttttatggc
EMSA_RNA	accauuaagcaugcgccgccugaaccacaccac/36-FAM
Crosslink_RNA	gucucucgacccaccuugcg
Pbu_Cas13b_crRNA_A	ggatatagcctggtggttcaggcggcgcatgcgttgcatctgccttctttttgaaaggtaaaaaca ac
Target_RNA_A	ggcacagccttatatcacacagcatgcgccgcctgaaccaccaggctatatcacacaatggaa ccatat

References and Notes

1. O. O. Abudayyeh, J. S. Gootenberg, S. Konermann, J. Joung, I. M. Slaymaker, D. B. T. Cox, S. Shmakov, K. S. Makarova, E. Semenova, L. Minakhin, K. Severinov, A. Regev, E. S. Lander, E. V. Koonin, F. Zhang, C2c2 is a single-component programmable RNA-guided RNA-targeting CRISPR effector. *Science* **353**, aaf5573 (2016).

2. A. East-Seletsky, M. R. O'Connell, S. C. Knight, D. Burstein, J. H. D. Cate, R. Tjian, J. A. Doudna, Two distinct RNase activities of CRISPR-C2c2 enable guide-RNA processing and RNA detection. *Nature* **538**, 270–273 (2016).

3. M. R. O'Connell, Molecular Mechanisms of RNA Targeting by Cas13-containing Type VI CRISPR-Cas Systems. *J. Mol. Biol.* **431**, 66–87 (2019).

4. A. J. Meeske, S. Nakandakari-Higa, L. A. Marraffini, Cas13-induced cellular dormancy prevents the rise of CRISPR-resistant bacteriophage. *Nature* **570**, 241–245 (2019).

5. A. A. Smargon, D. B. T. Cox, N. K. Pyzocha, K. Zheng, I. M. Slaymaker, J. S. Gootenberg, O. A. Abudayyeh, P. Essletzbichler, S. Shmakov, K. S. Makarova, E. V. Koonin, F. Zhang, Cas13b Is a Type VI-B CRISPR-Associated RNA-Guided RNase Differentially Regulated by Accessory Proteins Csx27 and Csx28. *Mol. Cell* **65**, 618–630.e7 (2017).

6. S. Shmakov, A. Smargon, D. Scott, D. Cox, N. Pyzocha, W. Yan, O. O. Abudayyeh, J. S. Gootenberg, K. S. Makarova, Y. I. Wolf, K. Severinov, F. Zhang, E. V. Koonin, Diversity and evolution of class 2 CRISPR-Cas systems. *Nat. Rev. Microbiol.* **15**, 169–182 (2017).

7. M. C. Pillon, J. Gordon, M. N. Frazier, R. E. Stanley, HEPN RNases - an emerging class of functionally distinct RNA processing and degradation enzymes. *Crit. Rev. Biochem. Mol. Biol.* **56**, 88–108 (2021).

8. H. Shivram, B. F. Cress, G. J. Knott, J. A. Doudna, Controlling and enhancing CRISPR systems. *Nat. Chem. Biol.* **17**, 10–19 (2021).

9. W. X. Yan, S. Chong, H. Zhang, K. S. Makarova, E. V. Koonin, D. R. Cheng, D. A. Scott, Cas13d Is a Compact RNA-Targeting Type VI CRISPR Effector Positively Modulated by a WYL-Domain-Containing Accessory Protein. *Mol. Cell* **70**, 327–339.e5 (2018).

10. V. Hoikkala, J. Ravantti, C. Díez-Villaseñor, M. Tiirola, R. A. Conrad, M. J. McBride, S. Moineau, L.-R. Sundberg, Cooperation between Different CRISPR-Cas Types Enables Adaptation in an RNA-Targeting System. *mBio* **12**, e03338-20 (2021).

11. N. Toro, M. R. Mestre, F. Martínez-Abarca, A. González-Delgado, Recruitment of Reverse Transcriptase-Cas1 Fusion Proteins by Type VI-A CRISPR-Cas Systems. *Front. Microbiol.* **10**, 2160 (2019).

12. S. Konermann, P. Lotfy, N. J. Brideau, J. Oki, M. N. Shokhirev, P. D. Hsu, Transcriptome Engineering with RNA-Targeting Type VI-D CRISPR Effectors. *Cell* **173**, 665–676.e14 (2018).

13. A. Krogh, B. Larsson, G. von Heijne, E. L. Sonnhammer, Predicting transmembrane protein topology with a hidden Markov model: Application to complete genomes. *J. Mol. Biol.* **305**, 567–580 (2001).

14. J. Syrjanen, K. Michalski, T. Kawate, H. Furukawa, On the molecular nature of large-pore channels. *J. Mol. Biol.* **433**, 166994 (2021).

15. L. Holm, L. M. Laakso, Dali server update. *Nucleic Acids Res.* **44** (W1), W351-W355 (2016).

16. M. van Kempen, S. S. Kim, C. Tumescheit, M. Mirdita, J. Söding, M. Steinegger , Foldseek: fast and accurate protein structure search. bioRxiv 2022.02.07.479398 [Preprint] (2022). https://doi.org/10.1101/2022.02.07.479398.

17. T. Aderinwale, V. Bharadwaj, C. Christoffer, G. Terashi, Z. Zhang, R. Jahandideh, Y. Kagaya, D. Kihara, Real-time structure search and structure classification for AlphaFold protein models. *Commun. Biol.* **5**, 316 (2022).

18. H. Suzuki, T. Kawabata, H. Nakamura, Omokage search: Shape similarity search service for biomolecular structures in both the PDB and EMDB. *Bioinformatics* **32**, 619–620 (2016).

19. V. Anantharaman, K. S. Makarova, A. M. Burroughs, E. V. Koonin, L. Aravind, Comprehensive analysis of the HEPN superfamily: Identification of novel roles in intra-genomic conflicts, defense, pathogenesis and RNA processing. *Biol. Direct* **8**, 15 (2013).

20. J. Jumper, R. Evans, A. Pritzel, T. Green, M. Figurnov, O. Ronneberger, K. Tunyasuvunakool, R. Bates, A. Žídek, A. Potapenko, A. Bridgland, C. Meyer, S. A. A. Kohl, A. J. Ballard, A. Cowie, B. Romera-Paredes, S. Nikolov, R. Jain, J. Adler, T. Back, S. Petersen, D. Reiman, E. Clancy, M. Zielinski, M. Steinegger, M. Pacholska, T. Berghammer, S. Bodenstein, D. Silver, O. Vinyals, A. W. Senior, K. Kavukcuoglu, P. Kohli, D. Hassabis, Highly accurate protein structure prediction with AlphaFold. *Nature* **596**, 583–589 (2021).

21. M. Baek, F. DiMaio, I. Anishchenko, J. Dauparas, S. Ovchinnikov, G. R. Lee, J. Wang, Q. Cong, L. N. Kinch, R. D. Schaeffer, C. Millán, H. Park, C. Adams, C. R. Glassman, A. DeGiovanni, J. H. Pereira, A. V. Rodrigues, A. A. van Dijk, A. C. Ebrecht, D. J. Opperman, T. Sagmeister, C. Buhlheller, T. Pavkov-Keller, M. K. Rathinaswamy, U. Dalwadi, C. K. Yip, J. E. Burke, K. C. Garcia, N. V. Grishin, P. D. Adams, R. J. Read, D. Baker, Accurate prediction of protein structures and interactions using a three-track neural network. *Science* **373**, 871–876 (2021).

22. R. Evans, M. O'Neill, A. Pritzel, N. Antropova, A. Senior, T. Green, A. Žídek, R. Bates, S. Blackwell, J. Yim, O. Ronneberger, S. Bodenstein, M. Zielinski, A. Bridgland, A. Potapenko, A. Cowie, K. Tunyasuvunakool, R. Jain, E. Clancy, P. Kohli, J. Jumper, D. Hassabis, Protein complex prediction with AlphaFold-Multimer. bioRxiv 2021.10.04.463034 [Preprint] (2022). https://doi.org/10.1101/2021.10.04.46303.

23. J. Stautz, Y. Hellmich, M. F. Fuss, J. M. Silberberg, J. R. Devlin, R. B. Stockbridge, I. Hänelt, Molecular Mechanisms for Bacterial Potassium Homeostasis. *J. Mol. Biol.* **433**, 166968 (2021).

24. J. D. Te Winkel, D. A. Gray, K. H. Seistrup, L. W. Hamoen, H. Strahl, Analysis of Antimicrobial-Triggered Membrane Depolarization Using Voltage Sensitive Dyes. *Front. Cell Dev. Biol.* **4**, 29 (2016).

25. F. M. Harold, J. Van Brunt, Circulation of H+ and K+ across the plasma membrane is not obligatory for bacterial growth. *Science* **197**, 372–373 (1977).

26. N. Kinoshita, T. Unemoto, H. Kobayashi, Proton motive force is not obligatory for growth of Escherichia coli. *J. Bacteriol.* **160**, 1074–1077 (1984).

27. E. W. Birch, N. A. Ruggero, M. W. Covert, Determining host metabolic limitations on viral replication via integrated modeling and experimental perturbation. *PLOS Comput. Biol.* **8**, e1002746 (2012).

28. O. Braissant, M. Astasov-Frauenhoffer, T. Waltimo, G. Bonkat, A Review of Methods to Determine Viability, Vitality, and Metabolic Rates in Microbiology. *Front. Microbiol.* **11**, 547458 (2020).

29. L. C. Thomason, D. L. Court, Evidence that bacteriophage λ lysogens may induce in response to the proton motive force uncoupler CCCP. *FEMS Microbiol. Lett.* **363**, fnv244 (2016).

30. I. Jain, M. Kolesnik, L. Minakhin, N. Morozova, A. Shiriaeva, A. Kirillov, S. Medvedeva, K. Kuznedelov, S. Borukhov, K. S. Makarova, E. V. Koonin, K. Severinov, E. Semenova, tRNA anticodon cleavage by target-activated CRISPR-Cas13a effector. bioRxiv 2021.11.10.468108 [Preprint] (2021). https://doi.org/10.1101/2021.11.10.468108.

31. J. L. Nieva, V. Madan, L. Carrasco, Viroporins: Structure and biological functions. *Nat. Rev. Microbiol.* **10**, 563–574 (2012).

32. L. M. R. Napolitano, V. Torre, A. Marchesi, CNG channel structure, function, and gating: A tale of conformational flexibility. *Pflugers Arch.* **473**, 1423–1435 (2021).

33. F. St-Pierre, D. Endy, Determination of cell fate selection during phage lambda infection. *Proc. Natl. Acad. Sci. U.S.A.* **105**, 20705–20710 (2008).

34. N. Bonilla, M. I. Rojas, G. Netto Flores Cruz, S.-H. Hung, F. Rohwer, J. J. Barr, Phage on tap-a quick and efficient protocol for the preparation of bacteriophage laboratory stocks. *PeerJ* **4**, e2261 (2016).

35. D. J. Slotboom, R. H. Duurkens, K. Olieman, G. B. Erkens, Static light scattering to characterize membrane proteins in detergent solution. *Methods* **46**, 73–82 (2008).

36. F. Wang, Y. Liu, Z. Yu, S. Li, S. Feng, Y. Cheng, D. A. Agard, General and robust covalently linked graphene oxide affinity grids for high-resolution cryo-EM. *Proc. Natl. Acad. Sci. U.S.A.* **117**, 24269–24273 (2020).

37. M. A. Herzik Jr., Setting Up Parallel Illumination on the Talos Arctica for High-Resolution Data Collection. *Methods Mol. Biol.* **2215**, 125–144 (2021).

38. D. N. Mastronarde, Automated electron microscope tomography using robust prediction of specimen movements. *J. Struct. Biol.* **152**, 36–51 (2005).

39. D. Tegunov, P. Cramer, Real-time cryo-electron microscopy data preprocessing with Warp. *Nat. Methods* **16**, 1146–1152 (2019).

40. A. Punjani, J. L. Rubinstein, D. J. Fleet, M. A. Brubaker, cryoSPARC: Algorithms for rapid unsupervised cryo-EM structure determination. *Nat. Methods* **14**, 290–296 (2017).

41. J. Zivanov, T. Nakane, B. O. Forsberg, D. Kimanius, W. J. H. Hagen, E. Lindahl, S. H. W. Scheres, New tools for automated high-resolution cryo-EM structure determination in RELION-3. *eLife* **7**, e42166 (2018).

42. J. Zivanov, T. Nakane, S. H. W. Scheres, A Bayesian approach to beam-induced motion correction in cryo-EM single-particle analysis. *IUCrJ* **6**, 5–17 (2019).

43. P. Emsley, B. Lohkamp, W. G. Scott, K. Cowtan, Features and development of Coot. *Acta Crystallogr. D Biol. Crystallogr.* **66**, 486–501 (2010).

44. E. F. Pettersen, T. D. Goddard, C. C. Huang, G. S. Couch, D. M. Greenblatt, E. C. Meng, T. E. Ferrin, UCSF Chimera—A visualization system for exploratory research and analysis. *J. Comput. Chem.* **25**, 1605–1612 (2004).

45. B. Frenz, A. C. Walls, E. H. Egelman, D. Veesler, F. DiMaio, RosettaES: A sampling strategy enabling automated interpretation of difficult cryo-EM maps. *Nat. Methods* **14**, 797–800 (2017).

46. B. A. Barad, N. Echols, R. Y.-R. Wang, Y. Cheng, F. DiMaio, P. D. Adams, J. S. Fraser, EMRinger: Side chain-directed model and map validation for 3D cryo-electron microscopy. *Nat. Methods* **12**, 943–946 (2015).

47. C. J. Williams, J. J. Headd, N. W. Moriarty, M. G. Prisant, L. L. Videau, L. N. Deis, V. Verma, D. A. Keedy, B. J. Hintze, V. B. Chen, S. Jain, S. M. Lewis, W. B. Arendall 3rd, J. Snoeyink, P. D. Adams, S. C. Lovell, J. S. Richardson, D. C. Richardson, MolProbity: More and better reference data for improved all-atom structure validation. *Protein Sci.* **27**, 293–315 (2018).

48. P. V. Afonine, B. P. Klaholz, N. W. Moriarty, B. K. Poon, O. V. Sobolev, T. C. Terwilliger, P. D. Adams, A. Urzhumtsev, New tools for the analysis and validation of cryo-EM maps and atomic models. *Acta Crystallogr. D Struct. Biol.* **74**, 814–840 (2018).

49. N. Echols, R. W. Grosse-Kunstleve, P. V. Afonine, G. Bunkóczi, V. B. Chen, J. J. Headd, A. J. McCoy, N. W. Moriarty, R. J. Read, D. C. Richardson, J. S. Richardson, T. C. Terwilliger, P. D. Adams, Graphical tools for macromolecular crystallography in PHENIX. *J. Appl. Crystallogr.* **45**, 581–586 (2012).

50. M. Mirdita, S. Ovchinnikov, M. Steinegger, ColabFold - Making protein folding accessible to all. *bioRxiv*, 2021.08.15.456425 [Preprint] (2021). https://doi.org/10.1101/2021.08.15.456425.

51. J. Hallgren, K. D. Tsirigos, M. D. Pedersen, J. J. Almagro Armenteros, P. Marcatili, H. Nielsen, A. Krogh, O. Winther, DeepTMHMM predicts alpha and beta transmembrane proteins using deep neural networks. *bioRxiv*, 2022.04.08.487609 [Preprint] (2022). https://doi.org/10.1101/2022.04.08.487609.

52. S. F. Altschul, T. L. Madden, A. A. Schäffer, J. Zhang, Z. Zhang, W. Miller, D. J. Lipman, Gapped BLAST and PSI-BLAST: A new generation of protein database search programs. *Nucleic Acids Res.* **25**, 3389–3402 (1997).

53. I. Letunic, P. Bork, Interactive Tree Of Life (iTOL) v5: An online tool for phylogenetic tree display and annotation. *Nucleic Acids Res.* **49**, W293–W296 (2021).

54. C. J. Jeffery, Expression, Solubilization, and Purification of Bacterial Membrane Proteins. *Curr. Protoc. Protein Sci.* **83**, 29.15.1–29.15.15 (2016).

55. E. Vialetto, Y. Yu, S. P. Collins, K. G. Wandera, L. Barquist, C. L. Beisel, A target expression threshold dictates invader defense and prevents autoimmunity by CRISPR-Cas13. *Cell Host Microbe* **30**, 1151–1162.e6 (2022).